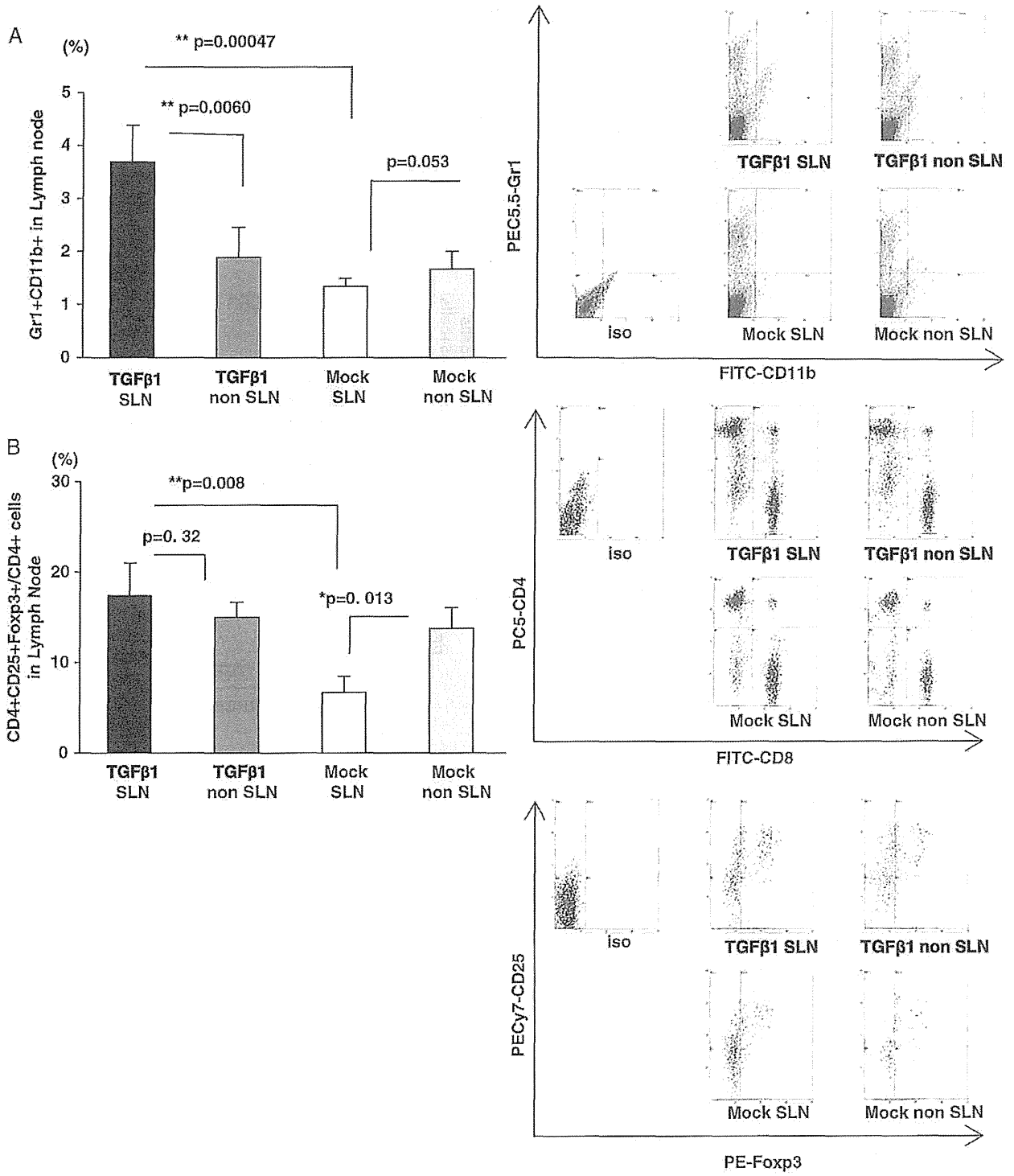

FIGURE 4. Tumor-derived TGF-β1 induces MDSCs and CD4+ Treg in SLNs. A and B, In the CT26-TGF-β1-bearing mice, the number of MDSCs and the percentage of Tregs in CD4+ T cells in SLNs significantly increased compared with CT26-MOCK-bearing mice. The number of MDSCs in SLNs was also higher than that of non-SLNs of the CT26-TGF-β1-bearing mice. The numbers of MDSCs and Tregs in SLNs of CT26-MOCK-bearing mice were reduced compared with non-SLNs. The data are representative of 3 independent experiments and shown as average ± SD. Representative FACS dot plots are shown for each bar graph.

primary tumors (Figs. 4A, B). The number of MDSCs in SLNs was also higher than that of non-SLNs in the CT26-TGF-β1-bearing mice, although significant increase of Tregs was not observed in SLNs compared with non-SLNs. It is interesting to note that, the numbers of MDSCs and Tregs in SLNs of the CT26-MOCK-bearing mice were reduced along with increase of DCs compared with non-SLNs (Figs. 4A, B, 5A), possibly suggesting induction of

antitumor immune responses when TGF-β1 level was low in tumor microenvironments in this relatively immunogenic CT26 mouse model. These results indicate that the overproduction of TGF-β1 by tumor cells in the tumor microenvironments generates immunosuppressive condition in SLNs through induction of immunosuppressive MDSCs and Tregs.

Overproduction of TGF-β1 Led to Impairment of DC Function in the SLNs

We then evaluated DCs in SLNs. The number of DCs in SLNs was significantly higher than non-SLNs in both CT26-TGF-β1 and CT26-MOCK-bearing mice (Fig. 5A). There was no significant difference in the number of DCs in SLNs between CT26-TGF-β1-bearing and CT26-MOCK-bearing mice. The DCs in SLNs showed significantly higher expression of CD80 compared with non-SLNs in CT26-MOCK-bearing mice (Fig. 5B). These observations may indicate the activation of DCs in SLNs particularly in CT26-MOCK-bearing mice along with the decrease of MDSCs and Tregs as shown in Figs. 4A, B. In contrast, in SLNs of CT26-TGF-β1-bearing mice, CD80 expression was not increased, MHC class II expression was decreased, and PD-L1$^+$CD11c$^+$ DCs were significantly higher compared with non-SLNs (Figs. 5B–D). Decrease of CD80 in DCs and increase of PD-L1$^+$ DCs were also observed in SLNs of CT26-TGF-β1-bearing mice compared with CT26-MOCK-bearing mice (Figs. 5B, D).

To evaluate functional difference of DCs in SLNs between CT26-TGF-β1-bearing mice and CT26-MOCK-bearing mice, the production of TNF-α by LPS-stimulated DCs and T-cell stimulatory activity of DCs in the presence of anti-CD3 mAb (MLR assay) were analyzed. TNF-α production ability and T-cell stimulatory activity of DCs in SLNs of CT26-TGF-β1-bearing mice was significantly decreased compared with DCs in SLNs of CT26-MOCK-bearing mice (Figs. 6A, B). It is interesting to note that, T-cell stimulatory activity of DCs of SLNs from the CT26-MOCK-bearing mice was significantly increased compared with the non-SLNs, suggesting the induction of antitumor immune responses as previously discussed with the observation of decrease of MDSCs and Tregs and increase of high MHC class II and CD80-expressing DCs (Figs. 4, 5). These results indicate that the tumor cell–derived TGF-β1 in the tumor microenvironments also induce immunosuppressive conditions in SLNs through the impairment of DCs and increase of MDSCs and Tregs.

Suppression of Tumor Antigen–specific CTL Induction in SLNs of TGF-β1-producing Tumors

Lastly, in vivo induction of tumor antigen–specific T cells from SLNs of CT26-TGF-β1-bearing and CT26-MOCK-bearing mice was evaluated. Six days after the tumor implantation, streptococcal preparation of OK432 which stimulates various TLRs was injected intratumorally, and 8 days later, cells from SLNs and non-SLNs of the CT26-TGF-β1-bearing and CT26-MOCK-bearing mice were stimulated in vitro with an immunodominant CT26 T-cell epitope peptide AH-1 for 8 days, and then induction of AH-1-specific T cells was evaluated by IFN-γ release assay. Although strong IFN-γ release was detected in the SLNs of CT26-MOCK-bearing mice compared with the non-SLNs, AH-1-specific T-cell response was almost undetectable in either SLNs or non-SLNs of CT26-TGF-β1-bearing mice (Fig. 6C). Therefore, induction of tumor antigen–specific CTLs seems to be inhibited in SLNs by immunosuppressive conditions caused by the TGF-β1 overexpression in tumor tissues.

DISCUSSION

In addition to systemic immunosuppression occurring at late stage of cancer patients, local immunosuppression in tumor-associated microenvironments including the tumor tissues and SLNs are critical for cancer progression. In this CT26 mouse tumor model, we were able to recapitulate the immunologic phenomena observed in the tumors and SLNs of cancer patients. Patients with high Treg accumulation in the SLNs showed poorer prognosis than those with low Treg accumulation in various cancers.[8,12,15–17] Tumor microenvironments are generally thought to be immunosuppressive through relative increase of Tregs, MDSCs, and M2 macrophages, and impairment of DC function. Here, we demonstrated that overproduction of TGF-β1 in tumor microenvironments promoted those immunosuppressive changes observed in cancer patients. The TGF-β1 overexpression in tumor microenvironments abrogated the possible spontaneous immune responses such as increased T-cell stimulatory activity of DCs along with high CD80 expression and decreased MDSCs and Tregs population in the SLNs. Infiltration of memory CD8$^+$ T cells in the tumors has recently been reported to correlate with good prognoses in various cancers.[1–3] The spontaneous CD8$^+$ T-cell response may also correlate with clinical responses to immunotherapy and chemotherapy.[4,5] Our study suggests that the elevation of immunosuppressive cytokines such as TGF-β1 in tumor microenvironments could be one of the mechanisms for immunosuppression in the SLNs and subsequent reduction of spontaneous CD8$^+$ T-cell responses among cancer patients, which are possibly associated with cancer patient's prognosis.

It has been reported in cancer patients that SLNs with no metastasis showed decreased number of DCs and downregulation of their HLA class II and costimulatory molecules.[7,18–20] In contrast, some studies showed increase of CD83$^+$-matured DCs in tumor-free SLNs compared with tumor-metastasized SLNs.[21] In our relatively immunogenic CT26 mouse tumor model, increase of DCs in tumor-free SLNs was observed in both CT26-MOCK-bearing and CT26-TGF-β1-bearing mice, suggesting that TGF-β1 had minimal effects on accumulation of DCs in the SLNs.

The differences of MDSCs in tumor-free SLNs and non-SLNs have not been investigated in patients with cancer.[22] In this study, we demonstrated that TGF-β1 in tumor microenvironments increased MDSC population in tumor-free SLNs. Although TGF-β1 has been reported to be one of the factors regulating MDSC activation,[23,24] it may not be directly involved in the recruitment of MDSCs into the SLNs. MDSC recruitments may be indirectly enhanced through chemokines such as CCL2 produced by TGF-β1-stimulated cells in the tumors or SLNs.

There have been several reports describing the relationship between TGF-β1 and immunologic condition of SLNs. Liu et al[25] reported that vaccination with TGF-β1 knock-out tumor cells induced better antitumor immune responses in SLNs and spleens, leading to improved antitumor effects, although they did not evaluate various immunosuppressive cells including MDSCs and DCs. Imai et al[26] reported that the migration of intratumorally

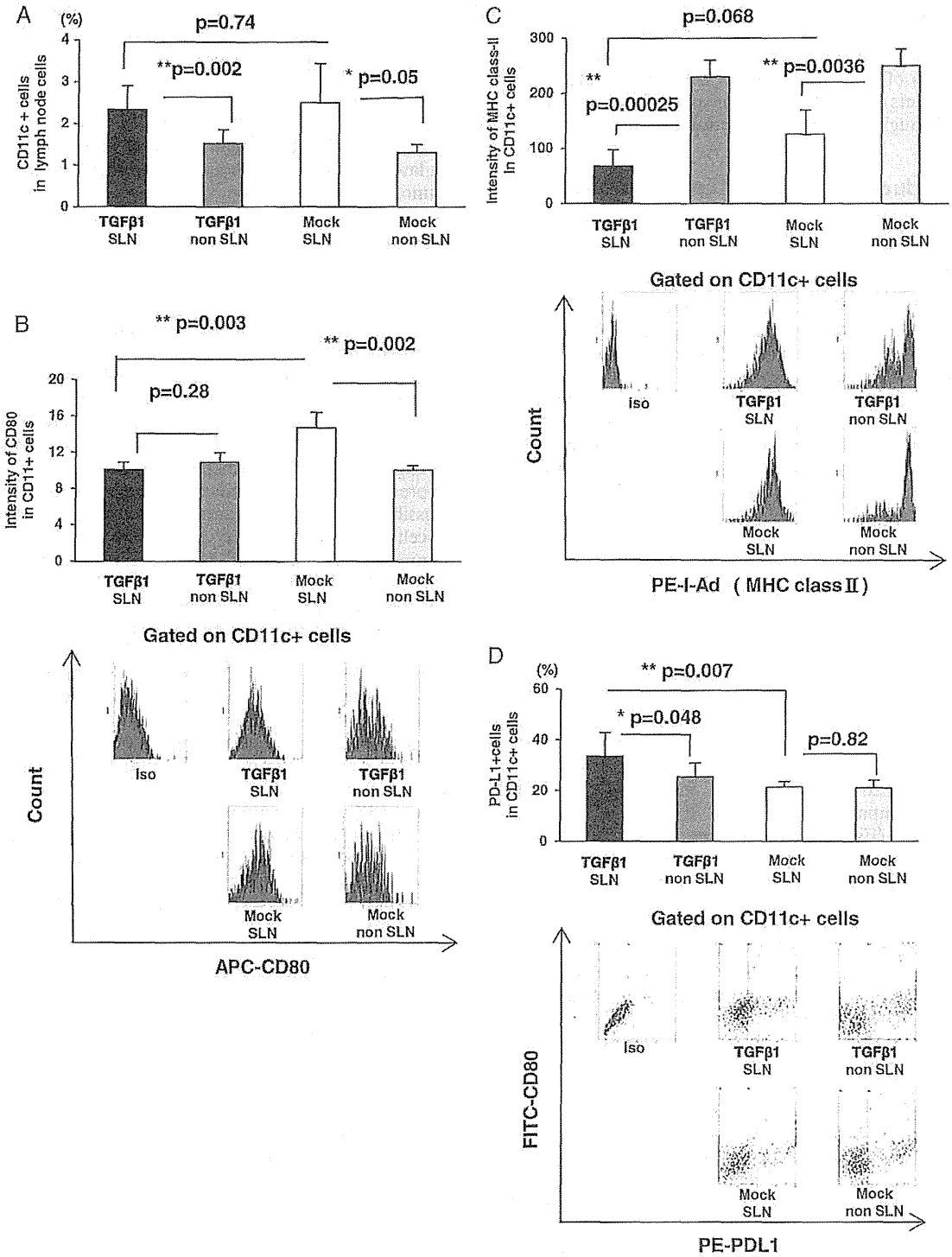

FIGURE 5. Tumor-derived TGF-β1 induces the immunosuppressive microenvironments in SLNs by inducing DCs with low CD80 and high PD-L1 expression. The number of DCs (A), expression levels of CD80 (B), and MHC class II (C) in DCs, and the proportion of PD-L1$^+$ cells in DCs (D) in SLNs or non-SLNs of CT26-TGF-β1-bearing mice or CT26-MOCK-bearing mice are shown. The data are representative of 3 independent experiments and shown as average ± SD. Representative FACS dot plots and histograms are shown for each bar graph.

injected DCs into the SLNs was reduced in mice implanted with TGF-β1-overexpressing tumors. Fujita et al[27] showed that the administration of plasmid DNA encoding TGF-β type-II receptor near tumor sites resulted in activation of tumor antigen–specific T cells and decreased Treg numbers in SLNs. Ito et al[18] showed increased DC apoptosis and

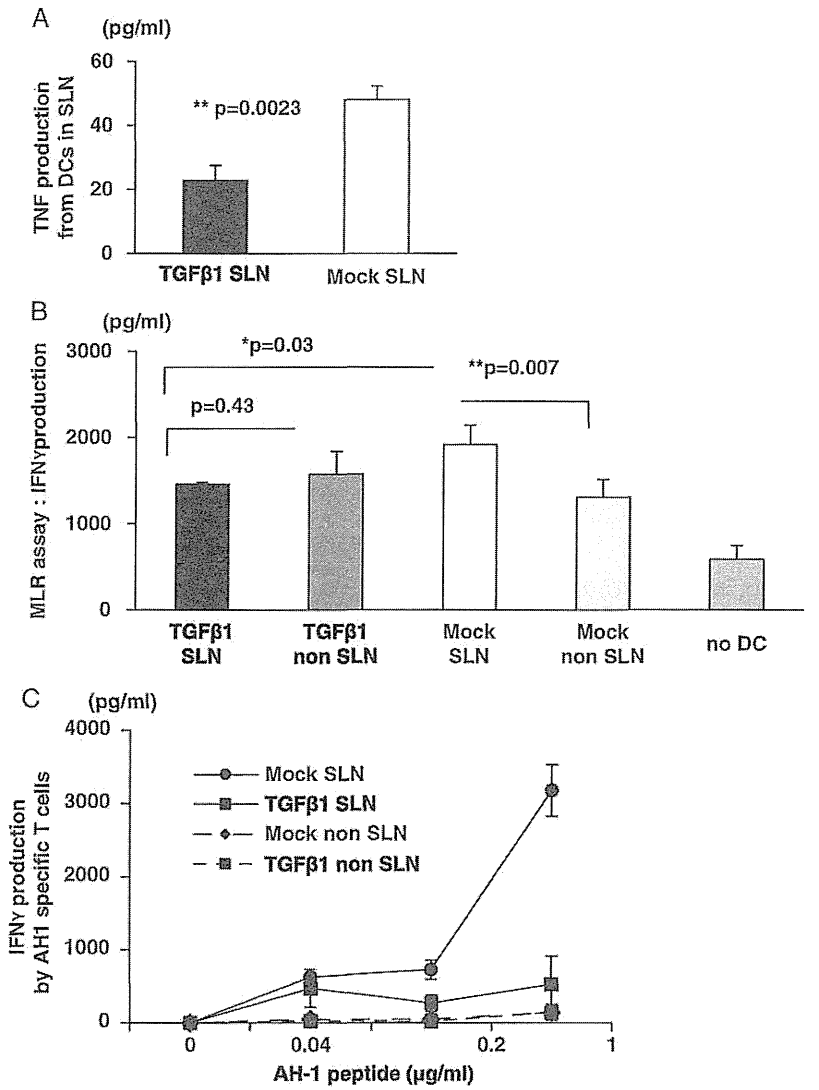

FIGURE 6. Suppressed DC function and impaired induction of tumor antigen–specific CTL in SLNs of CT26-TGF-β-bearing mice. A, DCs from the lymph nodes were stimulated with LPS (1 μg/mL) for 18 hours and TNF-α production was measured. B, DCs were irradiated and cocultured with T cells from Balb/c mice in the presence of anti-CD3-Ab for 4 days. IFN-γ production was determined to measure T-cell activation. T cells incubated without DCs (no DCs) serve as negative control. C, In vivo induction of tumor antigen–specific T cells from LNs of CT26-TGF-β1-bearing and CT26-MOCK-bearing mice was evaluated. Cells derived from SLNs or non-SLNs were restimulated in vitro with AH-1 peptide at a concentration of 1 μg/mL for 8 days. Then, 2×10^5 lymphocytes isolated from the culture were incubated with 1×10^6 MMC-treated syngeneic splenocytes in the presence of AH-1 peptides at various concentrations for 24 hours. Impaired IFN-γ production from CTL was observed in SLNs of CT26-TGF-β-bearing mice. The data are representative of 3 independent experiments and shown as average ± SD.

decrease of DC numbers in nonmetastasized SLNs of patients with non–small cell lung cancer by immunohistochemical and flow cytometric analysis. Gorelik et al[28] reported that TGF-β signaling in T cells inhibited Th1 differentiation and had negative effects on antitumor immune responses.[29] Immune suppressive effects of TGF-β1 in SLNs observed in our experiments might be partly due to the direct effects on T cells. These previous reports demonstrated various immunosuppressive roles of TGF-β1 in antitumor immune responses. These observations are in accord with the results of our study. However, we showed in this study a more comprehensive and simultaneous analysis of multiple immunologic changes including DCs, Tregs, MDSCs, and $CD8^+$ T cells, triggered by tumor-driven TGF-β1 in the microenvironments of both tumors and nonmetastasized SLNs, leading to better understanding of the role of TGF-β1 in the immunopathology of cancer, which may partially explain the difference of $CD8^+$ T-cell infiltration in tumors observed in various cancer patients.

Our study demonstrates that overexpression of TGF-β1 in tumor microenvironments drives immunosuppressive conditions in tumors and SLNs as observed in patients with various cancers. The TGF-β1 level in tumor microenvironments may determine the extent of spontaneous $CD8^+$ T-cell responses, which have been recently reported to correlate with good prognosis and response to various cancer treatments. TGF-β1 may be useful as a biomarker to

predict patients' prognosis and clinical response to cancer therapy. As TGF-β1 is also involved in tumor progression through various mechanisms including EMT induction, together with the results of this study, TGF-β1 pathway should be reemphasized as an attractive target for cancer treatment.

ACKNOWLEDGMENTS

The authors thank JeongHoon Park for preparation of the manuscript.

CONFLICTS OF INTEREST/ FINANCIAL DISCLOSURES

This work was supported by grants-in-aid for scientific research from the Ministry of Education, Culture, Sports, Science and Technology of Japan (23240128 and 24591635).

All authors have declared there are no financial conflicts of interest with regard to this work.

REFERENCES

1. Gajewski TF, Louahed J, Brichard VG. Gene signature in melanoma associated with clinical activity: a potential clue to unlock cancer immunotherapy. *Cancer J.* 2010;16:399–403.
2. Zhang L, Conejo-Garcia JR, Katsaros D, et al. Intratumoral T cells, recurrence, and survival in epithelial ovarian cancer. *N Engl J Med.* 2003;348:203–213.
3. Galon J, Costes A, Sanchez-Cabo F, et al. Type, density, and location of immune cells within human colorectal tumors predict clinical outcome. *Science.* 2006;313:1960–1964.
4. Galluzzi L, Senovilla L, Zitvogel L, et al. The secret ally: immunostimulation by anticancer drugs. *Nat Rev Drug Discov.* 2012;11:215–233.
5. Ladoire S, Mignot G, Dabakuyo S, et al. In situ immune response after neoadjuvant chemotherapy for breast cancer predicts survival. *J Pathol.* 2011;224:389–400.
6. Kohrt HE, Nouri N, Nowels K, et al. Profile of immune cells in axillary lymph nodes predicts disease-free survival in breast cancer. *PLoS Med.* 2005;2:e284.
7. Matsuura K, Yamaguchi Y, Ueno H, et al. Maturation of dendritic cells and T-cell responses in sentinel lymph nodes from patients with breast carcinoma. *Cancer.* 2006;106: 1227–1236.
8. Nakamura R, Sakakibara M, Nagashima T, et al. Accumulation of regulatory T cells in sentinel lymph nodes is a prognostic predictor in patients with node-negative breast cancer. *Eur J Cancer.* 2009;45:2123–2131.
9. Lee JH, Torisu-Itakara H, Cochran AJ, et al. Quantitative analysis of melanoma-induced cytokine-mediated immunosuppression in melanoma sentinel nodes. *Clin Cancer Res.* 2005; 11:107–112.
10. Lee JH, Chen Y, Chan JL, et al. Molecular analysis of melanoma-induced sentinel lymph node immune dysfunction. *Cancer Immunol Immunother.* 2011;60:685–692.
11. Cochran AJ, Huang RR, Lee J, et al. Tumour-induced immune modulation of sentinel lymph nodes. *Nat Rev Immunol.* 2006;6:659–670.
12. Deng L, Zhang H, Luan Y, et al. Accumulation of foxp3 + T regulatory cells in draining lymph nodes correlates with disease progression and immune suppression in colorectal cancer patients. *Clin Cancer Res.* 2010;16:4105–4112.
13. Yaguchi T, Sumimoto H, Kudo-Saito C, et al. The mechanisms of cancer immunoescape and development of overcoming strategies. *Int J Hematol.* 2011;93:294–300.
14. Sumimoto H, Imabayashi F, Iwata T, et al. The BRAF-MAPK signaling pathway is essential for cancer-immune evasion in human melanoma cells. *J Exp Med.* 2006;203: 1651–1656.
15. Mansfield AS, Heikkila PS, Vaara AT, et al. Simultaneous Foxp3 and IDO expression is associated with sentinel lymph node metastases in breast cancer. *BMC Cancer.* 2009;9:231.
16. Brody JR, Costantino CL, Berger AC, et al. Expression of indoleamine 2,3-dioxygenase in metastatic malignant melanoma recruits regulatory T cells to avoid immune detection and affects survival. *Cell Cycle.* 2009;8:1930–1934.
17. Knol AC, Nguyen JM, Quereux G, et al. Prognostic value of tumor-infiltrating Foxp3 + T-cell subpopulations in metastatic melanoma. *Exp Dermatol.* 2011;20:430–434.
18. Ito M, Minamiya Y, Kawai H, et al. Tumor-derived TGFbeta-1 induces dendritic cell apoptosis in the sentinel lymph node. *J Immunol.* 2006;176:5637–5643.
19. Cochran AJ, Morton DL, Stern S, et al. Sentinel lymph nodes show profound downregulation of antigen-presenting cells of the paracortex: implications for tumor biology and treatment. *Mod Pathol.* 2001;14:604–608.
20. Essner R, Kojima M. Dendritic cell function in sentinel nodes. *Oncology (Williston Park).* 2002;16:27–31.
21. Poindexter NJ, Sahin A, Hunt KK, et al. Analysis of dendritic cells in tumor-free and tumor-containing sentinel lymph nodes from patients with breast cancer. *Breast Cancer Res.* 2004;6: R408–R415.
22. Meyer C, Sevko A, Ramacher M, et al. Chronic inflammation promotes myeloid-derived suppressor cell activation blocking antitumor immunity in transgenic mouse melanoma model. *Proc Natl Acad Sci U S A.* 2011;108:17111–17116.
23. Lechner MG, Megiel C, Russell SM, et al. Functional characterization of human Cd33 + and Cd11b + myeloid-derived suppressor cell subsets induced from peripheral blood mononuclear cells co-cultured with a diverse set of human tumor cell lines. *J Transl Med.* 2011;9:90.
24. Gabrilovich DI, Nagaraj S. Myeloid-derived suppressor cells as regulators of the immune system. *Nat Rev Immunol.* 2009;9:162–174.
25. Liu P, Jaffar J, Zhou Y, et al. Inhibition of TGFβ1 makes nonimmunogenic tumor cells effective for therapeutic vaccination. *J Immunother.* 2009;32:232–239.
26. Imai K, Minamiya Y, Koyota S, et al. Inhibition of dendritic cell migration by transforming growth factor-beta1 increases tumor-draining lymph node metastasis. *J Exp Clin Cancer Res.* 2012;31:3.
27. Fujita T, Teramoto K, Ozaki Y, et al. Inhibition of transforming growth factor-beta-mediated immunosuppression in tumor-draining lymph nodes augments antitumor responses by various immunologic cell types. *Cancer Res.* 2009;69: 5142–5150.
28. Gorelik L, Constant S, Flavell RA. Mechanism of transforming growth factor β-induced inhibition of T helper type1 differentiation. *J Exp Med.* 2002;195:1499–1505.
29. Gorelik L, Flavell RA. Immune-mediated eradication of tumors through the blockade of transforming factor-β signaling in T cells. *Nat Med.* 2001;7:1118–1122.

RESEARCH PAPER

Cancer Biology & Therapy 15:1, 81–88; January 2014; © 2014 Landes Bioscience

Continuous low-dose irradiation by I-125 seeds induces apoptosis of gastric cancer cells regardless of histological origin

Kaoru Takabayashi[1], Kazuhiro Kashiwagi[2], Tetsuya Kawata[3], Toshiro Sato[1], Katsuyoshi Matsuoka[1], Tadakazu Hisamatsu[1], Hiromasa Takaishi[4], Toshifumi Hibi[1], Haruhiko Ogata[2], Naohisa Yahagi[5], Yuko Kitagawa[6], Naoyuki Shigematsu[3], and Takanori Kanai[1,*]

[1]Division of Gastroenterology and Hepatology; Department of Internal Medicine; School of Medicine; Keio University; Tokyo, Japan; [2]Center for Diagnostic and Therapeutic Endoscopy; School of Medicine; Keio University; Tokyo, Japan; [3]Department of Radiology; School of Medicine; Keio University; Tokyo, Japan; [4]Cancer Center; School of Medicine; Keio University; Tokyo, Japan; [5]Division of Research and Development for Minimally Invasive Treatment; Cancer Center; School of Medicine; Keio University; Tokyo, Japan; [6]Department of Surgery; School of Medicine; Keio University; Tokyo, Japan

Keywords: I-125 seed irradiation, gastric cancer, apoptosis, cell cycle, caspase

The efficacy of conventional radiation therapy for gastric cancer is controversial. In this study, we evaluated the in vitro and in vivo effects of continuous low-dose-rate irradiation by I-125 seeds on different histological types of gastric cancer cell lines. Three human gastric cancer cell lines (MKN74, MKN45, and NUGC4) were treated with or without continuous low-dose irradiation by I-125 seeds in vitro and in vivo. Cell viability, apoptosis, caspase-3 assay, and cell-cycle distribution were examined in vitro. Body weight and tumor volumes of BALB/c nude mice bearing MKN74, MKN45, and NUGC4 gastric cancer xenografts were measured, and in vivo cell proliferation and apoptosis assays were performed by Ki67 and TUNEL staining, respectively. Continuous low-dose-rate irradiation by I-125 seeds reduced cell viability and induced cell apoptosis through the activation of caspase-3, and led to the accumulation of cells in the G_2/M phase in vitro. It also suppressed the growth of gastric cancer xenografts in nude mice, while inhibiting cell proliferation and inducing apoptosis as demonstrated by Ki67 and TUNEL staining. Therefore, our data suggest that continuous low-dose-rate irradiation by I-125 seeds could be a promising new option for gastric cancer treatment, regardless of histological origin.

Introduction

Gastric cancer is the fourth most frequent malignancy and the second leading cause of cancer-related mortality in the world.[1] Although the incidence of gastric cancer has been decreasing, it remains a common malignancy worldwide, especially in Asia.[2,3] Endoscopic submucosal dissection has recently emerged as a common treatment for early-stage IA gastric cancer,[4,5] while surgical resection remains a standard therapeutic approach for early gastric cancer. However, for stages III and IV advanced gastric cancers, surgical treatment alone is not regarded as the definitive standard treatment. This is because the 5-y survival rates of stages III and IV patients were reported to be less than 50% even when a curative operation was performed.[6,7] The high rate of relapse after surgical treatment makes it important to consider adjuvant treatment for patients with advanced gastric cancer. Several studies of chemotherapy for advanced gastric cancer were reported, but adjuvant chemotherapy has not resulted in higher survival rates than surgical treatment alone. As a result, chemoradiotherapy is being evaluated as an alternate treatment for gastric cancer.

Several studies, including the clinical trial INT0116,[8] have reported that postoperative chemoradiotherapy could be a powerful treatment for controlling tumor progression in advanced gastric cancer.[9-11] This led to the inclusion of radiotherapy as a standard treatment for patients with a high risk of recurrence[12-14] in the National Comprehensive Cancer Network (NCCN) guidelines on gastric cancer treatment. Therefore, in the USA and Europe, postoperative chemoradiotherapy has becoming a standard treatment for advanced gastric cancer. However, there are some drawbacks of radiation therapy for gastric cancer. These include the difficulty of establishing the area to irradiate because of peristaltic movement, complications affecting the surrounding organs, risk of perforation and ulceration by high-dose radiation, and ineffectiveness against adenocarcinoma with low radiosensitivity. Therefore, in Japan, radiation therapy has not been established as a standard treatment for advanced gastric cancer. Indications for radiation therapy are limited, and it is performed only as a palliative therapy.[15-17] Because of this, more effective and safer therapeutic strategies for advanced or unresectable gastric cancer are expected.

In recent years, I-125 seed implantation providing continuous low-dose-rate irradiation has been widely used to treat prostate cancer and other kinds of tumors in several Asian countries because of little trauma, strong effect, and fewer complications,[18-21]

*Correspondence to: Takanori Kanai; Email: takagast@z2.keio.jp
Submitted: 08/06/2013; Revised: 09/11/2013; Accepted: 09/25/2013
http://dx.doi.org/10.4161/cbt.26610

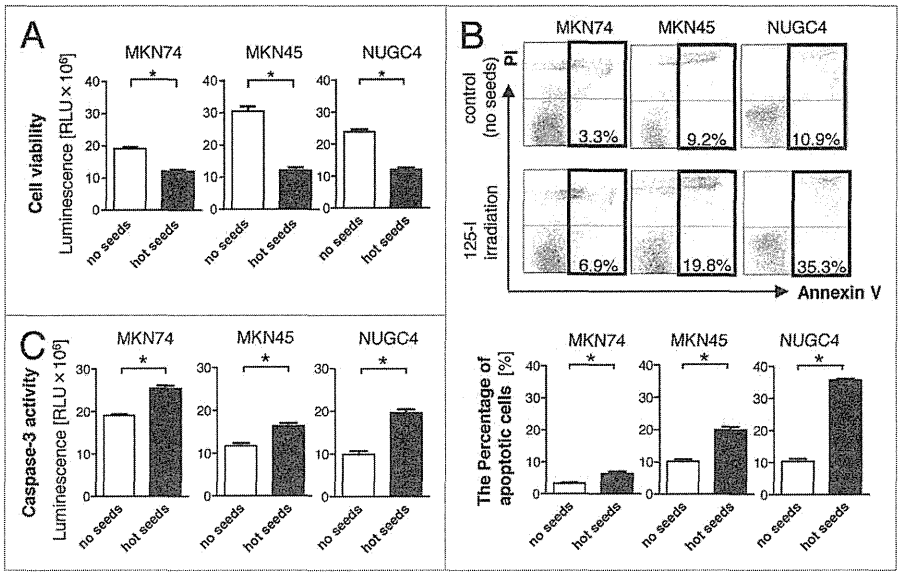

Figure 1. Cell viability of the three gastric cancer cell lines (MKN74, MKN45, and NUGC4) was assessed following incubation for 96 h with or without irradiation to maintain constant cell culture conditions. The viability of each of the 3 cell lines was significantly lower than that of the control group (*$P < 0.05$) (**A**). Apoptosis was determined by flow cytometry and the total apoptosis rate was calculated. The total apoptosis rate induced by irradiation was significantly increased in each of the three gastric cancer cell lines as compared with the control (*$P < 0.05$) (representative data was shown in [**B**]). Caspase-3 assay was performed and the activity of caspase-3 was increased significantly in all 3 irradiated gastric cancer cell lines ($P < 0.05$) (**C**). Experiments were performed at least 3 times.

while in Japan, I-125 seed implantation therapy is provided only for prostate cancer. In this study, we investigate the effect of continuous low-dose-rate irradiation by I-125 seeds on several types of gastric cancer in vitro and in vivo to determine its potential as a novel therapeutic strategy for advanced and unresectable gastric cancer.

Results

I-125 seeds reduced cell viability and induced cell apoptosis in vitro

To determine the direct effects of I-125 seeds in gastric cancer cell lines, three gastric cancer cell lines (MKN74, MKN45, and NUGC4) were assayed after treatment with (2–3 Gy) or without (0 Gy, no seeds as a control) irradiation. Cell viability was significantly lower than in the control group in each of the three gastric cancer cell lines following irradiation ($P < 0.05$) (**Fig. 1A**). To analyze the induction of apoptosis by irradiation, double staining of cells with annexin V-FITC and propidium iodide (PI) was performed. Annexin V-positive/PI-negative cell staining was considered to denote early apoptosis, while annexin V/PI-double-positive cell staining was considered to denote late apoptosis (**Fig. 1B**). **Figure 1B** shows the total apoptosis rate (annexin V-positive rate) in all cell lines. The total apoptosis rate induced by irradiation was significantly increased in each of the three gastric cancer cell lines as compared with the control ($P < 0.05$). Recent studies have identified caspases, including caspase-3, as important mediators of apoptosis induced by various apoptotic stimuli.[22] The activity of caspase-3 was significantly increased in all irradiated gastric cancer cell lines ($P < 0.05$) (**Fig. 1C**), thus confirming that I-125 seed irradiation caused apoptosis in gastric cancer cells through the activation of caspase-3.

I-125 seeds reduced cell-cycle arrest in vitro

The results of the flow cytometry cell-cycle assay (**Fig. 2A and B**) indicated that the continuous low-dose-rate irradiation by I-125 seeds induced a lower percentage of G_0/G_1, and higher percentage of G_2/M phase cell-cycle arrest in all three cell lines compared with the control, and the differences were statistically significant ($P < 0.05$). These results suggest that continuous low-dose-rate irradiation by I-125 seeds may enhance radiosensitivity by inducing accumulation of cells in the more radiosensitive G_2/M phase.

I-125 seeds inhibited tumor growth of gastric cancer in vivo

Tumor xenografts consisting of transplanted human gastric cancer cell lines MKN45 (derived from poorly differentiated adenocarcinoma) or NUGC4 (derived from signet-ring cell carcinoma) were used to evaluate the antitumor effects of I-125 seeds in vivo (**Fig. 3A**, data not shown for NUGC4). When tumors of both cell lines reached around 400 mm^3 at day 28, cold and hot seeds were implanted. Tumors which I-125 seeds were implanted were smaller rather than cold seeds or the control at day 52 (**Fig. 3B**). There were no significant changes in tumor volumes during the first 2 weeks after seed implantation, but after that, I-125 irradiated tumors were significantly smaller than the non-irradiated tumors ($P < 0.05$) (**Fig. 3C**). This indicated that I-125 seeds significantly inhibited tumor growth during the 3- to 4-week treatment. As shown in **Figure 3D**, the body weights of mice were not affected by the I-125 irradiation. Besides, none of the mice died during the treatment, and no obvious radiation-induced damage was observed in vital organs (data not shown). These results underscore the safety of I-125 seed treatment.

I-125 seeds inhibited cell proliferation and induced apoptosis in vivo

To quantitatively compare the proliferation and apoptotic rates, MKN45 and NUGC4 xenograft tumor sections were taken from mice in the control, cold seed, and I-125 seed implanted groups, and immunostained for Ki67 and TUNEL. In addition, before immunostaining, cells were isolated as described, stained with annexin V-FITC and PI, and analyzed using a flow cytometer to clarify the induction of apoptosis. There were

clearly fewer Ki67-positive cells in the I-125 seed implanted group than in the control and cold seed implanted groups (**Fig. 4A and B**). In contrast to the proliferation rate, the average number of TUNEL-positive apoptotic cells in the I-125 seed implanted group was significantly increased compared with the control and cold seed implanted groups ($P < 0.05$). The apoptosis rate (annexin V-positive staining as determined by flow cytometry) in the I-125 implanted group was significantly increased over that of the control and cold seed implanted groups ($P < 0.05$) (**Fig. 4C**). These results suggested that I-125 seeds inhibited cell proliferation and induced apoptosis in MKN45 and NUGC4 xenografts.

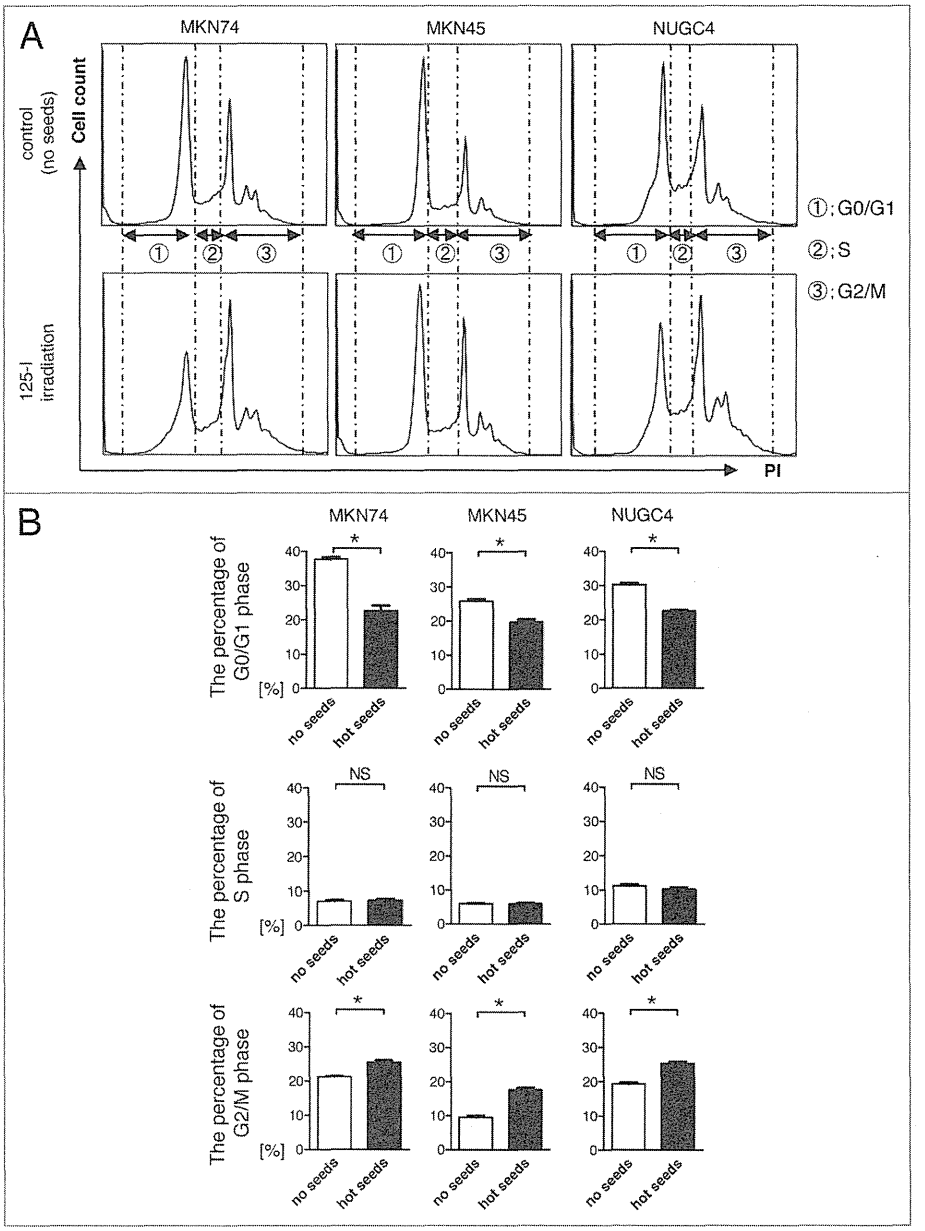

Figure 2. Cell-cycle assay was performed on each of the three gastric cancer cell lines (MKN74, MKN45, and NUGC4) following incubation for 96 h with or without irradiation to maintain constant cell culture conditions (representative data was shown in [**A**]). Three cell-cycle segments are shown in order from left to right: G_1/G_0 phase, S phase, G_2/M phase, and the percentage of cells in each phase is shown in (**B**). Continuous low-dose-rate irradiation by I-125 seeds induced a lower percentage of G_0/G_1, and higher percentage of G_2/M phase cell-cycle arrest compared with the control for all 3 gastric cancer cell lines ($P < 0.05$). Experiments were performed at least 3 times.

Discussion

Gastric cancer remains a major cause of death in the world. Radiation therapy has recently started to play an important role in the treatment of advanced gastric cancer. However, the adverse effects of conventional external beam radiation therapy on surrounding organs pose a major problem. With recent technological advances in irradiation, e.g., intensity-modulated radiation therapy, irradiation is localized to the restricted area as far as possible. However, adverse effects remain a problem. In this study, we examined the effectiveness of I-125 seed irradiation therapy to address this problem. As described above, I-125 seeds serve as a localized radiation source with an irradiation range of <2 cm. If the seeds can provide the same therapeutic effects for gastric cancer in a more localized irradiated region than conventional external beam radiation therapy, then they may serve as a new radiation therapy, which reduces the adverse effects of radiation on the surrounding organs.

According to a recent report, continuous low-dose-rate irradiation by I-125 seeds plays an important role in apoptosis induction and cell-cycle arrest. However, this remains controversial[18,23] and, moreover, this was reported in only one histological type of gastric cancer or cancer of other organs[24-27] Undifferentiated cancer cells are generally more sensitive to radiation. Thus, radiation effects may vary with cancer histology. Therefore, three histologically different gastric cancer cell lines (well to moderately differentiated adenocarcinoma, poorly differentiated adenocarcinoma, and signet-ring cell carcinoma) were tested in vitro and in vivo in our study.

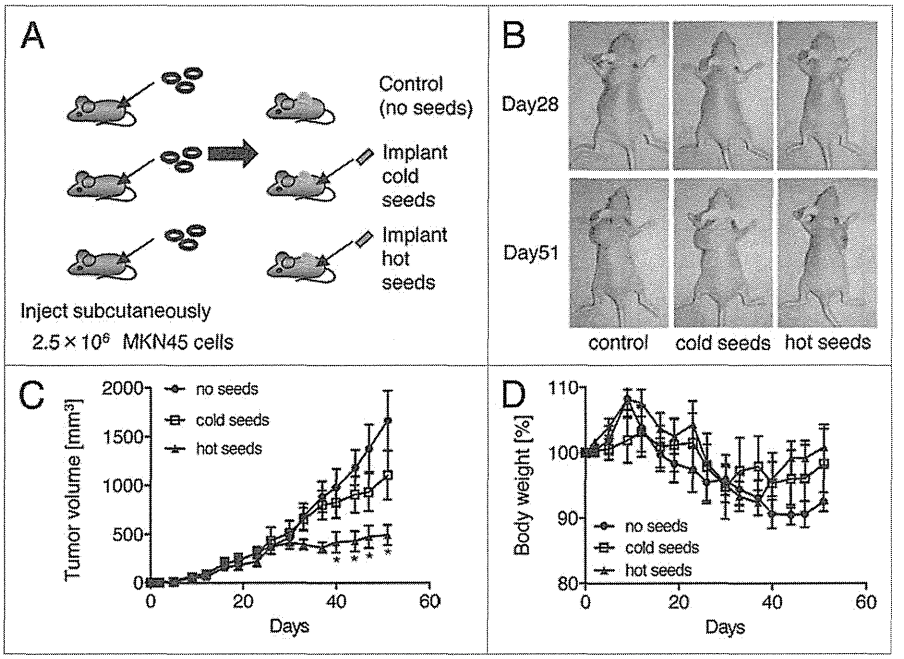

Figure 3. Protocol for animal experiments using the MKN45 cell line (**A**). 2.5 × 10^6 cells in 0.2 ml PBS were injected subcutaneously into the dorsa of each mouse. When tumors reached around 400 mm^3 at about 3–4 weeks, I-125 seeds or cold seeds were implanted into each 5 mice per group via a needle. The untreated mice served as the no seed control group. The tumor's macroscopic appearance was imaged on the day of implantation before the mouse was sacrificed (representative data was shown in [**B**]). Tumor size was measured once every 4 d. There were no significant changes in tumor volume during the first 2 weeks after seed implantation, but after that, I-125-irradiated tumors were much smaller than the others, and significant differences in tumor volumes were observed between the I-125 seed implanted group and the other 2 groups ($P < 0.05$) (**C**). The body weight of the animals was also measured every 4 d and mortality was monitored daily, but there were no significant differences between the 3 groups (**D**).

Our results demonstrated that I-125 irradiation reduced cell viability and activated caspase-3 to induce apoptosis in all histological types. Apoptosis induction rates tended to be higher for poorly differentiated cells, although no significant difference was noted.

Apoptosis is a specific form of cell death characterized by several morphological and biochemical events.[28,29] Apoptosis plays an important role in a wide variety of biological processes including immune system and homeostatic system development.[30] Atypical cells that survive by inhibiting apoptosis are expected to contribute to tumor progression and oncogenesis, and cancer cells often gain a selective growth advantage by blocking apoptosis. Therefore, we hypothesized that induction of apoptotic cell death must be an important mechanism in the anticancer properties of I-125 irradiation.

Cell-cycle analysis demonstrated that I-125 irradiation significantly decreased cells in the G_0/G_1 phase and increased cells in the G_2/M phase. It is well recognized that the radiation sensitivity of cells is highest in the G_2/M phase.[31,32] Our results also demonstrated that I-125 irradiation inhibited the G_2 to M phase transition during the cell cycle, delaying cell division through the accumulation of cells in the G_2/M phase to enhance cell radiosensitivity in all histological types of gastric cancer in vitro. Furthermore, I-125 irradiation impairs the cell's ability to repair the damage, thereby promoting cell apoptosis, which is consistent with our data.

A subsequent study using a subcutaneous implantation model of gastric cancer cells demonstrated that tumor growth was significantly suppressed only in the I-125 seed implanted group. Subsequent Ki67 and TUNEL staining demonstrated that I-125 irradiation significantly suppressed the proliferation of cancer and induced apoptosis in the residual tumors within the non-necrotic regions. These results suggest that the I-125 irradiation-induced cell death was caused by both necrosis and apoptosis in all three histological types of gastric cancer in vivo.

Thus, I-125 irradiation caused radiation-induced cell death in tumors, but did not significantly damage subcutaneous tissue and intra-abdominal organs in this experiment. Over the course of the study, the body weights of the mice did not significantly differ and all the mice survived, suggesting that I-125 irradiation is safe with few complications. Sugawara et al.[33] conducted a study of patients with I-125 seeds that had migrated to a site other than the prostate among 267 patients who underwent brachytherapy for prostate cancer. The I-125 seeds leaked directly into the abdominal and pelvic cavities and migrated to the lungs, gastrointestinal tract, and kidneys through the bloodstream. However, none of the patients suffered serious complications, demonstrating that I-125 irradiation therapy is very safe. The late adverse effects of radiation and administration methods for hollow organs should be further investigated.

In conclusion, I-125 seed irradiation exerts anti-tumor effects by inducing apoptosis and suppressing proliferation in histologically varied gastric cancers (adenocarcinoma and signet-ring cell carcinoma). Thus, I-125 irradiation can serve as a novel radiation therapy for gastric cancer, with minimal adverse effects on the surrounding organ.

Materials and Methods

Cell culture

Three gastric cancer cell lines (MKN74, MKN45, and NUGC4), kindly provided by RIKEN BRC Cell Bank through the National Bio-Resource Project of the Ministry of Education,

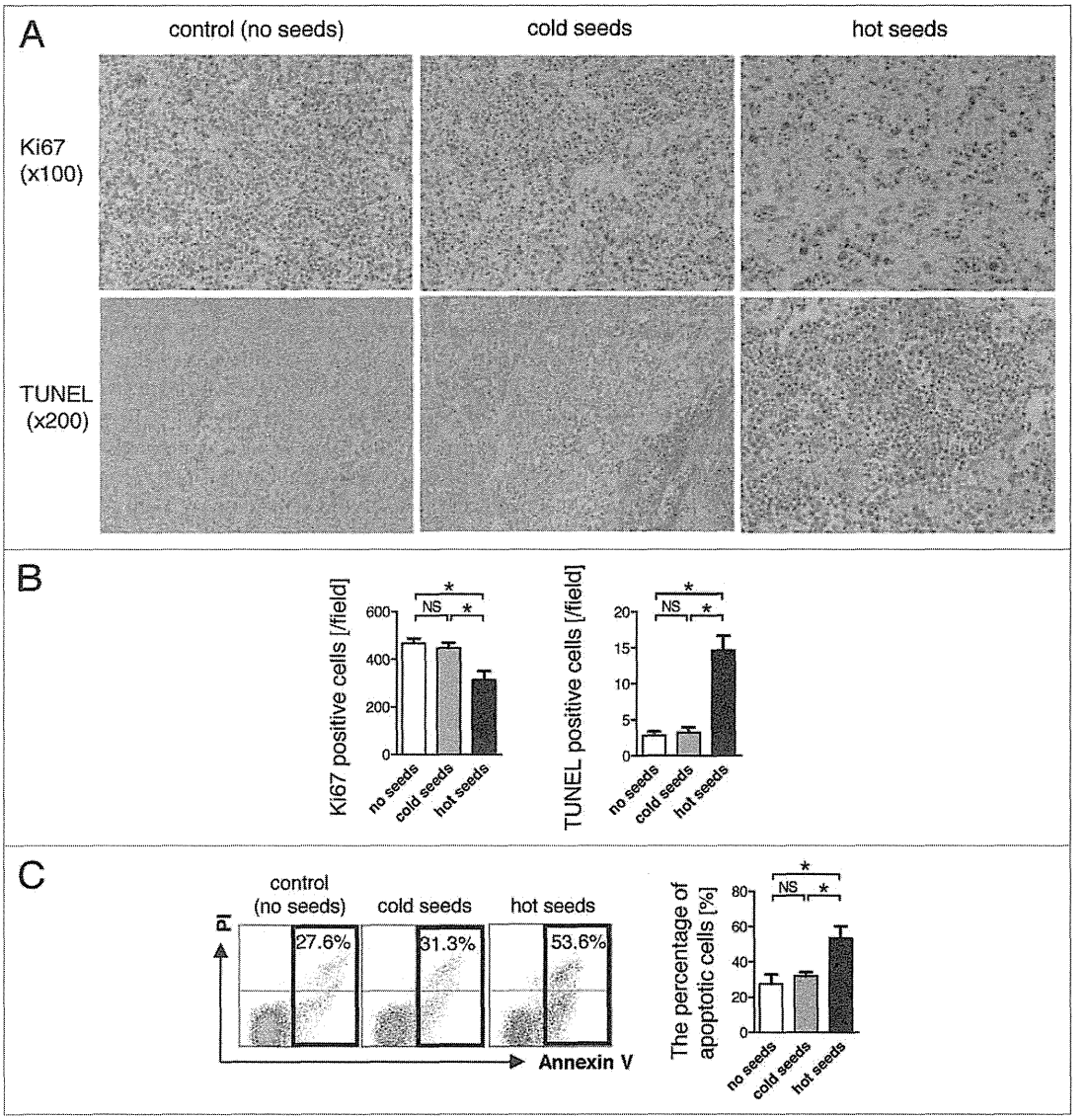

Figure 4. Histological experiments with MKN45 xenografts. Tumor sections were immunostained for Ki67 and a TUNEL assay was performed. Ki67 and TUNEL immunostaining are shown at 100× and 200× magnification (representative data was shown in [**A**]). Ki67 and TUNEL-positive cells were quantified in 20 randomly selected, high-power fields in each tissue section. The average number of Ki67-positive cells in the I-125 implanted group was clearly less than those in the control and cold seed implanted groups. In contrast to the proliferation rate, the average number of TUNEL-positive apoptotic cells in the I-125 implanted group was significantly increased over those in the control and cold seed implanted groups (*$P < 0.05$) (**B**). Tumor tissue samples were isolated and stained with annexin V-FITC and PI, then analyzed using a flow cytometer to clarify the induction of apoptosis. The apoptosis rate in the I-125 implanted group was significantly increased compared with those of the control and cold seed implanted groups ($P < 0.05$) (representative data was shown in [**C**]).

Culture, Sports, Science and Technology, Japan, were used in this study. MKN74 was derived from differentiated adenocarcinoma, MKN45 from poorly differentiated adenocarcinoma, and NUGC4 from signet-ring cell carcinoma. Cells were cultured in a RPMI 1640 (Invitrogen, Life Technologies Corp.) medium supplemented with 10% heat-inactivated fetal bovine serum (FBS), 100 U/ml penicillin, and 100 μg/ml streptomycin (Invitrogen, Life Technologies Corp.) at 37 °C in a 95%/5% humidified mixture of atmospheric air and CO_2.

I-125 seed irradiation model in vitro

Model 6711 I-125 seeds were kindly provided by GE Healthcare Medi-Physics, Inc.. The seeds were 0.97 mm in diameter, 4.55 mm long, with a surface activity of 15.3 MBq, a half-life of 59.4 d, and average energy of 27.4–35.5 Kev. We used our in-house in vitro I-125 seed irradiation model as described previously with minor modifications.[34,35] Parafilm® (Pechiney Plastic Packaging Company) was laid on the bottom of a 6-cm diameter cell culture dish. Eight I-125 seeds were evenly embedded

within recesses (4.55 mm × 0.97 mm) around a 35-mm diameter circumference, with one I-125 seed placed in the center of the 6-cm dish, to obtain a relatively homogeneous dose distribution at the surface of the cell culture dish. A 6-cm culture dish was placed on the in-house I-125 irradiation model during the experiment. From each cell line (MKN74, MKN45, and NUGC4), 1×10^5 cells were seeded into separate dishes, and incubated for 96 h under constant cell culture conditions. The culture dishes were rotated clockwise at specific time intervals to guarantee even irradiation of the cells. The cultured cells were divided into two groups: control group (0 Gy, without the embedded seeds), and I-125 seed irradiated group (described as hot seeds).

Preparation of cells for further experiments

Cells from the control and I-125 seed irradiated groups were digested with trypsin and gently washed with a serum-containing medium followed by a phosphate-buffered saline (PBS) wash. After that, cells were centrifuged at 190 × g for 5 min. The supernatant was discarded, and the cells were resuspended for counting.

Viability assay

Cell viability was assessed with the CellTiter-Glo® assay (Promega).[36] Cells were added to a 96-well plate (opaque-walled multi-well plates) at 2×10^5 cells per well in 100 μL media, and control wells containing only the medium were prepared to measure background luminescence. One hundred microliters of CellTiter-Glo® reagent was added to each well and the contents were mixed for 2 min on an orbital shaker to induce cell lysis. The plate was incubated at room temperature for 10 min. Data were then recorded using a plate-reading fluorometer Infinite® F200 PRO (Tecan Group Ltd.). Experiments were performed at least three times to ensure reproducibility.

Apoptosis analysis by flow cytometry

Cell concentrations were adjusted to 2×10^5 cells/ml for apoptosis analysis by flow cytometry. Cell suspensions were centrifuged at 190 × g for 5 min, and supernatants were discarded. Apoptosis assay was performed using the MEBCYTO® Apoptosis Kit (AnnexinV-FITC Kit) (Medical and Biological Laboratories Co, Ltd.)[37] for flow cytometry as described by the manufacturer. Cells were resuspended in 85 μL of binding buffer, followed by the addition of 10 μL of annexin V-FITC and 5 μL of propidium iodide, mixed well and incubated at room temperature (20–25 °C) for 15 min in the dark. After 100 μL of binding buffer was added, stained cells were analyzed using a flow cytometer (FACS Canto II; Becton Dickinson) and the data were analyzed using FlowJo software (Tree Star Inc.). Experiments were performed at least 3 times to ensure reproducibility.

Caspase-3 activity assay

Caspase-3 activity was assessed with the Caspase-Glo® 3/7 assay (Promega).[38] Cells were added to a 96-well plate (opaque-walled multi-well plates) at 2×10^5 cells per well in 100 μL media, and control wells containing only the medium were prepared to measure background luminescence. One hundred microliters of Caspase-Glo® reagent was added to each well and contents were mixed for 2 min on an orbital shaker to induce cell lysis. The plate was incubated at room temperature for 30 min. Data were then recorded using a plate-reading fluorometer Infinite® F200 PRO (TECAN Group Ltd.). Experiments were performed at least three times to ensure reproducibility.

Cell-cycle analysis by flow cytometry

Cell-cycle assay was performed using the Cell Cycle Phase Determination Kit® (Cayman Chemical Company)[39] for flow cytometry according to the manufacturer's instructions. The cell concentration was adjusted to 1×10^6 cells/ml for cell-cycle analysis by flow cytometry. Cell suspensions were centrifuged at 190 × g for 5 min, and supernatants were discarded. Cells were washed with an assay buffer twice, and then fixed and permeabilized with fixation solution at -20 °C overnight. The fixed cells were centrifuged at 500 × g for 5 min, and the fixation solution was discarded. The cell pellet was suspended in 0.5 ml staining solution (200 μL RNase A with 200 μL PI, 10 ml assay buffer), and incubated for 30 min at room temperature in the dark. The DNA content was determined by flow cytometry (FACS Canto II, Becton Dickinson) and the data were analyzed using FlowJo software (Tree Star Inc.). Experiments were performed at least three times to ensure reproducibility.

Animal experiments

Female BALB/c nude mice, 35–42 d old and weighing 17–20 g, were purchased from CLEA Japan, Inc. Mice were maintained under specific pathogen-free conditions in the Animal Care Facility of Keio University School of Medicine. All experiments were approved by the regional animal study committee and were performed according to institutional guidelines and home office regulations. Animals were anesthetized via inhalation of diethyl ether and 2.5×10^6 MKN45, or NUGC4 cells in 0.2 ml PBS was injected subcutaneously into the dorsa of each mouse. When tumors reached around 400 mm^3 at about 4 weeks, the mice were randomly assigned to 3 groups (n = 5/group). The visible mass in mice from two of the groups was punctured by the 18-gauge needles of the Mick-applicator through which I-125 seeds or cold seeds were implanted. The remaining group served as the non-implanted control group. Tumor size was measured once every 4 d, and expressed as tumor volume using the formula: tumor volume (mm^3) = (major axis) × (minor axis) × (height) × 0.52. The body weight of the animals was measured once every 4 d and mortality was monitored daily. After the treatment, all mice were sacrificed and weighed, and tumors were harvested and weighed.

Isolation of tumor cells from tumor xenografts

Tumor cells were isolated from tumors as described previously[40,41] with minor modifications. Briefly, tumors were cut into fragments 2–3 mm in width, and incubated in a RPMI 1640 medium containing 10% FBS, collagenase type I (300 U/ml; invitrogen, Life Technologies Corp.) and DNase I (50 U/ml; Sigma-Aldrich Corp.) at 37 °C for 90 min. Thereafter, the digested fragments were teased through a steel mesh and single-cell suspensions were resuspended in 40% Percoll (Biochrome) and layered over 75% Percoll prior to centrifugation at 500 × g for 45 min. Interphase tumor cells were stained with the MEBCYTO® Apoptosis Kit (AnnexinV-FITC Kit) (Medical and Biological Laboratories Co, Ltd.) for flow cytometry analysis.

Ki67 and TUNEL staining of tumor samples

Tumor samples were fixed in PBS containing 10% neutral-buffered formalin. For the detection of apoptotic cells, tissue

sections were subjected to a TUNEL assay using the In Situ Cell Death Detection Kit (Roche) according to the manufacturer's instructions. Cell proliferation was assessed by quantitative morphometric analysis of proliferating cell nuclear antigen (Ki67) expression. Tissue sections were deparaffinized with xylene, rehydrated with graded ethanol, and fixed in 4% paraformaldehyde. The tissue sections were incubated in an EDTA pH 9.0 buffer solution at 95 °C for 20 min and 0.3% H_2O_2 for 3–5 min. The slides were washed three times in PBS and incubated for 60 min at room temperature with a mouse monoclonal Ki67 antibody (Thermo Fisher Scientific, Inc.) at a 1:100 dilution. After that, slides were washed three times in Tris-buffered saline (TBS), and incubated for 30 min at room temperature with a peroxidase-conjugated anti-mouse IgG polyclonal antibody (Nichirei Bioscience Inc.). The Ki67 stain was visualized with a DAB substrate system in which nuclei with DNA fragmentation were stained brown. Ki67- or TUNEL-positive cells were quantified in 20 randomly selected, high-power fields (200×) of each tissue section.

Statistical analysis

Statistical analysis was performed with GraphPad Prism software (version 4.0; GraphPad Software, Inc.). Results were expressed as mean ± standard error of the mean. Groups of data were analyzed by ANOVA followed by the Tukey post hoc test. Differences were considered to be statistically significant when the *P* value was less than 0.05.

Disclosure of Potential Conflicts of Interest

No potential conflicts of interest were disclosed.

References

1. Herszényi L, Tulassay Z. Epidemiology of gastrointestinal and liver tumors. Eur Rev Med Pharmacol Sci 2010; 14:249-58; PMID:20496531
2. Roder DM. The epidemiology of gastric cancer. Gastric Cancer 2002; 5(Suppl 1):5-11; PMID:12772880; http://dx.doi.org/10.1007/s10120-002-0203-6
3. Terry MB, Gaudet MM, Gammon MD. The epidemiology of gastric cancer. Semin Radiat Oncol 2002; 12:111-27; PMID:11979413; http://dx.doi.org/10.1053/srao.30814
4. Hoteya S, Yahagi N, Iizuka T, Kikuchi D, Kawano K, Noguchi T, Mizuno H, Hashimoto M. [Endoscopic resection for early gastric cancers by EMR/ESD]. Gan To Kagaku Ryoho 2007; 34:16-20; PMID:17220663
5. Hoteya S, Yamashita S, Kikuchi D, Nakamura M, Fujimoto A, Matsui A, Nishida N, Mitani T, Kuroki Y, Iizuka T, et al. Endoscopic submucosal dissection for submucosal invasive gastric cancer and curability criteria. Dig Endosc 2011; 23:30-6; PMID:21198914; http://dx.doi.org/10.1111/j.1443-1661.2010.01040.x
6. Hundahl SA, Phillips JL, Menck HR. The National Cancer Data Base Report on poor survival of U.S. gastric carcinoma patients treated with gastrectomy: Fifth Edition American Joint Committee on Cancer staging, proximal disease, and the "different disease" hypothesis. Cancer. 2000;88: 921-932.
7. Landry J, Tepper JE, Wood WC, Moulton EO, Koerner F, Sullinger J. Patterns of failure following curative resection of gastric carcinoma. Int J Radiat Oncol Biol Phys 1990; 19:1357-62; PMID:2262358; http://dx.doi.org/10.1016/0360-3016(90)90344-J
8. Macdonald JS, Smalley SR, Benedetti J, Hundahl SA, Estes NC, Stemmermann GN, Haller DG, Ajani JA, Gunderson LL, Jessup JM, et al. Chemoradiotherapy after surgery compared with surgery alone for adenocarcinoma of the stomach or gastroesophageal junction. N Engl J Med 2001; 345:725-30; PMID:11547741; http://dx.doi.org/10.1056/NEJMoa010187
9. Ajani JA, Winter K, Okawara GS, Donohue JH, Pisters PW, Crane CH, Greskovich JF, Anne PR, Bradley JD, Willett C, et al. Phase II trial of preoperative chemoradiation in patients with localized gastric adenocarcinoma (RTOG 9904): quality of combined modality therapy and pathologic response. J Clin Oncol 2006; 24:3953-8; PMID:16921048; http://dx.doi.org/10.1200/JCO.2006.06.4840
10. Saikawa Y, Kubota T, Kumagai K, Nakamura R, Kumai K, Shigematsu N, Kubo A, Kitajima M, Kitagawa Y. Phase II study of chemoradiotherapy with S-1 and low-dose cisplatin for inoperable advanced gastric cancer. Int J Radiat Oncol Biol Phys 2008; 71:173-9; PMID:17996385; http://dx.doi.org/10.1016/j.ijrobp.2007.09.010
11. Takahashi T, Saikawa Y, Kubota T, Akiba Y, Shigematsu N, Yoshida M, Otani Y, Kumai K, Hibi T, Kitajima M. Histological complete response in a case of advanced gastric cancer treated by chemotherapy with S-1 plus low-dose cisplatin and radiation. Jpn J Clin Oncol 2003; 33:584-8; PMID:14711984; http://dx.doi.org/10.1093/jjco/hyg110
12. National Comprehensive Cancer Network. NCCN practice guidelines for upper gastrointestinal carcinomas. [Williston Park]. Oncology (Williston Park) 1998; 12(11A):179-223; PMID:10028512
13. Smalley SR, Gunderson L, Tepper J, Martenson JA Jr., Minsky B, Willett C, Rich T. Gastric surgical adjuvant radiotherapy consensus report: rationale and treatment implementation. Int J Radiat Oncol Biol Phys 2002; 52:283-93; PMID:11872272; http://dx.doi.org/10.1016/S0360-3016(01)02646-3
14. Zhang ZX, Gu XZ, Yin WB, Huang GJ, Zhang DW, Zhang RG. Randomized clinical trial on the combination of preoperative irradiation and surgery in the treatment of adenocarcinoma of gastric cardia (AGC)--report on 370 patients. Int J Radiat Oncol Biol Phys 1998; 42:929-34; PMID:9869212; http://dx.doi.org/10.1016/S0360-3016(98)00280-6
15. Yoshikawa T, Tsuburaya A, Hirabayashi N, Yoshida K, Nagata N, Kodera Y, Takahashi N, Oba K, Kimura M, Ishikura S, et al. A phase I study of palliative chemoradiation therapy with paclitaxel and cisplatin for local symptoms due to an unresectable primary advanced or locally recurrent gastric adenocarcinoma. Cancer Chemother Pharmacol 2009; 64:1071-7; PMID:19283353; http://dx.doi.org/10.1007/s00280-009-0963-3
16. Hashimoto K, Mayahara H, Takashima A, Nakajima TE, Kato K, Hamaguchi T, Ito Y, Yamada Y, Kagami Y, Itami J, et al. Palliative radiation therapy for hemorrhage of unresectable gastric cancer: a single institute experience. J Cancer Res Clin Oncol 2009; 135:1117-23; PMID:19205735; http://dx.doi.org/10.1007/s00432-009-0553-0
17. Asakura H, Hashimoto T, Harada H, Mizumoto M, Furutani K, Hasuike N, Matsuoka M, Ono H, Boku N, Nishimura T. Palliative radiotherapy for bleeding from advanced gastric cancer: is a schedule of 30 Gy in 10 fractions adequate? J Cancer Res Clin Oncol 2011; 137:125-30; PMID:20336314; http://dx.doi.org/10.1007/s00432-010-0866-z
18. Zhuang HQ, Wang JJ, Liao AY, Wang JD, Zhao Y. The biological effect of 125I seed continuous low dose rate irradiation in CL187 cells. J Exp Clin Cancer Res 2009; 28:12; PMID:19175942; http://dx.doi.org/10.1186/1756-9966-28-12
19. Yu Y, Anderson LL, Li Z, Mellenberg DE, Nath R, Schell MC, Waterman FM, Wu A, Blasko JC. Permanent prostate seed implant brachytherapy: report of the American Association of Physicists in Medicine Task Group No. 64. Med Phys 1999; 26:2054-76; PMID:10535622; http://dx.doi.org/10.1118/1.598721
20. Wang JJ, Yuan HS, Li JN, Jiang WJ, Jiang YL, Tian SQ. Interstitial permanent implantation of 125I seeds as salvage therapy for re-recurrent rectal carcinoma. Int J Colorectal Dis 2009; 24:391-9; PMID:19084969; http://dx.doi.org/10.1007/s00384-008-0628-4
21. Joyce F, Burcharth F, Holm HH, Strøyer I. Ultrasonically guided percutaneous implantation of iodine-125 seeds in pancreatic carcinoma. Int J Radiat Oncol Biol Phys 1990; 19:1049-52; PMID:1698755; http://dx.doi.org/10.1016/0360-3016(90)90032-F
22. Debatin KM. Apoptosis pathways in cancer and cancer therapy. Cancer Immunol Immunother 2004; 53:153-9; PMID:14749900; http://dx.doi.org/10.1007/s00262-003-0474-8
23. Wang J, Wang J, Liao A, Zhuang H, Zhao Y. The direct biologic effects of radioactive 125I seeds on pancreatic cancer cells PANC-1, at continuous low-dose rates. Cancer Biother Radiopharm 2009; 24:409-16; PMID:19694575; http://dx.doi.org/10.1089/cbr.2008.0563
24. Qiu H, Yashiro M, Shinto O, Matsuzaki T, Hirakawa K. DNA methyltransferase inhibitor 5-aza-CdR enhances the radiosensitivity of gastric cancer cells. Cancer Sci 2009; 100:181-8; PMID:19037991; http://dx.doi.org/10.1111/j.1349-7006.2008.01004.x
25. Marples B, Wouters BG, Collis SJ, Chalmers AJ, Joiner MC. Low-dose hyper-radiosensitivity: a consequence of ineffective cell cycle arrest of radiation-damaged G2-phase cells. Radiat Res 2004; 161:247-55; PMID:14982490; http://dx.doi.org/10.1667/RR3130
26. Carlsson J, Håkansson E, Eriksson V, Grawe J, Wester K, Grusell E, Montelius A, Lundqvist H. Early effects of low dose-rate radiation on cultured tumor cells. Cancer Biother Radiopharm 2003; 18:663-70; PMID:14503962; http://dx.doi.org/10.1089/108497803322287754
27. Mirzaie-Joniani H, Eriksson D, Johansson A, Löfroth PO, Johansson L, Ahlström KR, Stigbrand T. Apoptosis in HeLa Hep2 cells is induced by low-dose, low-dose-rate radiation. Radiat Res 2002; 158:634-40; PMID:12385641; http://dx.doi.org/10.1667/0033-7587(2002)158[0634:AIHHCI]2.0.CO;2
28. Hengartner MO. The biochemistry of apoptosis. Nature 2000; 407:770-6; PMID:11048727; http://dx.doi.org/10.1038/35037710

29. Saraste A, Pulkki K. Morphologic and biochemical hallmarks of apoptosis. Cardiovasc Res 2000; 45:528-37; PMID:10728374; http://dx.doi.org/10.1016/S0008-6363(99)00384-3
30. Meier P, Finch A, Evan G. Apoptosis in development. Nature 2000; 407:796-801; PMID:11048731; http://dx.doi.org/10.1038/35037734
31. Collis SJ, Schwaninger JM, Ntambi AJ, Keller TW, Nelson WG, Dillehay LE, Deweese TL. Evasion of early cellular response mechanisms following low level radiation-induced DNA damage. J Biol Chem 2004; 279:49624-32; PMID:15377658; http://dx.doi.org/10.1074/jbc.M409600200
32. Nakamura H, Yasui Y, Saito N, Tachibana A, Komatsu K, Ishizaki K. DNA repair defect in AT cells and their hypersensitivity to low-dose-rate radiation. Radiat Res 2006; 165:277-82; PMID:16494515; http://dx.doi.org/10.1667/RR3519.1
33. Sugawara A, Nakashima J, Kunieda E, Nagata H, Mizuno R, Seki S, Shiraishi Y, Kouta R, Oya M, Shigematsu N. Incidence of seed migration to the chest, abdomen, and pelvis after transperineal interstitial prostate brachytherapy with loose (125)I seeds. Radiat Oncol 2011; 6:130; PMID:21974959; http://dx.doi.org/10.1186/1748-717X-6-130
34. Ma JX, Jin ZD, Si PR, Liu Y, Lu Z, Wu HY, Pan X, Wang LW, Gong YF, Gao J, et al. Continuous and low-energy 125I seed irradiation changes DNA methyltransferases expression patterns and inhibits pancreatic cancer tumor growth. J Exp Clin Cancer Res 2011; 30:35; PMID:21457568; http://dx.doi.org/10.1186/1756-9966-30-35
35. Chen H, Bao Y, Yu L, Jia R, Cheng W, Shao C. Comparison of cellular damage response to low-dose-rate 125I seed irradiation and high-dose-rate gamma irradiation in human lung cancer cells. Brachytherapy 2012; 11:149-56; PMID:21664878; http://dx.doi.org/10.1016/j.brachy.2011.05.002
36. Crouch SP, Kozlowski R, Slater KJ, Fletcher J. The use of ATP bioluminescence as a measure of cell proliferation and cytotoxicity. J Immunol Methods 1993; 160:81-8; PMID:7680699; http://dx.doi.org/10.1016/0022-1759(93)90011-U
37. Ohara M, Hayashi T, Kusunoki Y, Nakachi K, Fujiwara T, Komatsuzawa H, Sugai M. Cytolethal distending toxin induces caspase-dependent and -independent cell death in MOLT-4 cells. Infect Immun 2008; 76:4783-91; PMID:18644882; http://dx.doi.org/10.1128/IAI.01612-07
38. Nicholson DW, Thornberry NA. Caspases: killer proteases. Trends Biochem Sci 1997; 22:299-306; PMID:9270303; http://dx.doi.org/10.1016/S0968-0004(97)01085-2
39. Sulić S, Panić L, Dikić I, Volarević S. Deregulation of cell growth and malignant transformation. Croat Med J 2005; 46:622-38; PMID:16100767
40. Kim M, Miyamoto S, Yasui Y, Oyama T, Murakami A, Tanaka T. Zerumbone, a tropical ginger sesquiterpene, inhibits colon and lung carcinogenesis in mice. Int J Cancer 2009; 124:264-71; PMID:19003968; http://dx.doi.org/10.1002/ijc.23923
41. Ju SA, Park SM, Lee YS, Bae JH, Yu R, An WG, Suh JH, Kim BS. Administration of 6-gingerol greatly enhances the number of tumor-infiltrating lymphocytes in murine tumors. Int J Cancer 2012; 130:2618-28; PMID:21792901; http://dx.doi.org/10.1002/ijc.26316

HEPATOLOGY
Official Journal of the American Association for the Study of Liver Diseases

Free Cholesterol Accumulation in Hepatic Stellate Cells: Mechanism of Liver Fibrosis Aggravation in Nonalcoholic Steatohepatitis in Mice

Kengo Tomita,[1,2]* Toshiaki Teratani,[2]* Takahiro Suzuki,[2] Motonori Shimizu,[1] Hirokazu Sato,[1] Kazuyuki Narimatsu,[1] Yoshikiyo Okada,[1] Chie Kurihara,[1] Rie Irie,[3] Hirokazu Yokoyama,[4] Katsuyoshi Shimamura,[2] Shingo Usui,[1,2] Hirotoshi Ebinuma,[2] Hidetsugu Saito,[5] Chikako Watanabe,[1] Shunsuke Komoto,[1] Atsushi Kawaguchi,[1] Shigeaki Nagao,[1] Kazuo Sugiyama,[2] Ryota Hokari,[1] Takanori Kanai,[2] Soichiro Miura,[1] and Toshifumi Hibi[2]

Although nonalcoholic steatohepatitis (NASH) is associated with hypercholesterolemia, the underlying mechanisms of this association have not been clarified. We aimed to elucidate the precise role of cholesterol in the pathophysiology of NASH. C57BL/6 mice were fed a control, high-cholesterol (HC), methionine-choline-deficient (MCD), or MCD+HC diet for 12 weeks or a control, HC, high-fat (HF), or HF+HC diet for 24 weeks. Increased cholesterol intake accelerated liver fibrosis in both the mouse models without affecting the degree of hepatocellular injury or Kupffer cell activation. The major causes of the accelerated liver fibrosis involved free cholesterol (FC) accumulation in hepatic stellate cells (HSCs), which increased Toll-like receptor 4 protein (TLR4) levels through suppression of the endosomal-lysosomal degradation pathway of TLR4, and thereby sensitized the cells to transforming growth factor (TGF)β-induced activation by down-regulating the expression of bone morphogenetic protein and activin membrane-bound inhibitor. Mammalian-cell cholesterol levels are regulated by way of a feedback mechanism mediated by sterol regulatory element-binding protein 2 (SREBP2), maintaining cellular cholesterol homeostasis. Nevertheless, HSCs were sensitive to FC accumulation because the high intracellular expression ratio of SREBP cleavage-activating protein (Scap) to insulin-induced gene (Insig) disrupted the SREBP2-mediated feedback regulation of cholesterol homeostasis in these cells. HSC activation subsequently enhanced the disruption of the feedback system by Insig-1 down-regulation. In addition, the suppression of peroxisome proliferator-activated receptor γ signaling accompanying HSC activation enhanced both SREBP2 and microRNA-33a signaling. Consequently, FC accumulation in HSCs increased and further sensitized these cells to TGFβ-induced activation in a vicious cycle, leading to exaggerated liver fibrosis in NASH. *Conclusion*: These characteristic mechanisms of FC accumulation in HSCs are potential targets to treat liver fibrosis in liver diseases including NASH. (HEPATOLOGY 2014;59:154-169)

Abbreviations: ABCA1, adenosine triphosphate-binding cassette A1; ALT, alanine aminotransferase; Bambi, bone morphogenetic protein and activin membrane-bound inhibitor; CCl_4, carbon tetrachloride; CE, cholesterol ester; COPII, coat protein complex II; ER, endoplasmic reticulum; FBS, fetal bovine serum; FC, free cholesterol; HC, high cholesterol; HF, high fat; HMGCR, 3-hydroxy-3-methyl-glutaryl-CoA reductase; HSC, hepatic stellate cell; ICAM-1, intercellular adhesion molecule-1; Insig, insulin-induced gene; LDLR, low-density lipoprotein receptor; LPS, lipopolysaccharide; Mβ CD, methyl-β-cyclodextrin; MCD, methionine-choline deficient; mRNA, messenger RNA; NASH, nonalcoholic steatohepatitis; NPC1, Niemann-Pick C1; PCR, polymerase chain reaction; PPAR, peroxisome proliferator-activated receptor; Scap, SREBP cleavage-activating protein; siRNA, small interfering RNA; SMA, smooth muscle actin; SREBP, sterol regulatory element-binding protein; TGF, transforming growth factor; TLR4, Toll-like receptor 4; TNF, tumor necrosis factor; TUNEL, terminal deoxynucleotidyl transferase-mediated deoxyuridine nick-end labeling; VCAM-1, vascular cell adhesion molecule-1.

From the [1]Division of Gastroenterology and Hepatology, Department of Internal Medicine, National Defense Medical College, Saitama, Japan; [2]Division of Gastroenterology and Hepatology, Department of Internal Medicine, Keio University School of Medicine, Tokyo, Japan; [3]Department of Pathology, Kawasaki Municipal Hospital, Kanagawa, Japan; [4]Health Center, Keio University School of Medicine, Tokyo, Japan; [5]Graduate School of Pharmaceutical Sciences, Keio University Faculty of Pharmacy, Tokyo, Japan.

Nonalcoholic steatohepatitis (NASH) is a progressive disease that can cause cirrhosis or liver-related complications.[1] It very often accompanies lifestyle diseases including hypercholesterolemia. Several studies have shown that statins and ezetimibe (cholesterol-lowering agents) improve liver fibrosis in patients with NASH.[2] Furthermore, we have recently reported that free cholesterol (FC) accumulation in hepatic stellate cells (HSCs) plays an important role in the pathogenesis of liver fibrosis.[3] These results drew our attention to the role of cholesterol in the pathogenesis of liver fibrosis in NASH.

Cholesterol homeostasis is tightly regulated by way of a feedback system mediated by sterol regulatory element-binding protein (SREBP)2.[4,5] The low-density lipoprotein receptor (LDLR) and 3-hydroxy-3-methylglutaryl-CoA reductase (HMGCR), which play important roles in maintaining cholesterol uptake and synthesis, respectively, are predominantly regulated by SREBP2.[6] Nascent SREBP2 localizes to the endoplasmic reticulum (ER) membrane and forms tight complexes with SREBP cleavage-activating protein (Scap), a membrane-embedded escort protein.[7] When membrane cholesterol levels are low, the SREBP2-Scap complex is incorporated into the coat protein complex II (COPII)-coated vesicles.[6,8] Consequently, SREBP2 translocates to the nucleus and activates transcription of several target genes involved in the biosynthesis and uptake of cholesterol.[6] When excess cholesterol accumulates in the ER membranes, it changes Scap to an alternate conformation, allowing it to bind to resident ER proteins, insulin-induced gene (Insig)-1, and Insig-2.[9] This binding precludes the binding of COPII. Consequently, the SREBP2-Scap complex remains in the ER, transcription of the target genes declines, and cholesterol synthesis and uptake fall.[4,6]

Furthermore, recent studies have shown that the primary transcript of SREBP2 also encodes miR-33a, a microRNA that regulates cholesterol metabolism by way of factors such as adenosine triphosphate-binding cassette A1 (ABCA1) and Niemann-Pick C1 (NPC1), suggesting transcriptional regulation by *SREBF2* modulates the cellular capacity for producing not only an active transcription factor but also the expression of miR-33a.[10]

By studying two mouse models of NASH, we attempted to clarify the precise role of cholesterol in the pathophysiology of NASH. As we found that the major causes of the exacerbation of liver fibrosis in NASH involved FC accumulation in HSCs, we investigated the underlying mechanisms of FC accumulation in HSCs and its role in the pathogenesis of NASH.

Materials and Methods

Please refer to the Supporting Materials and Methods for more detailed descriptions.

Reagents. Reagents were obtained as follows: low density lipoprotein (LDL), methyl-β-cyclodextrin (MβCD)/cholesterol complex, lipopolysaccharide (LPS), chloroquine, and MG-132 were from Sigma (St. Louis, MO). 25-HC was from Wako Pure Chemical Industries (Osaka, Japan). Transforming growth factor beta (TGFβ) was from R&D Systems (Minneapolis, MN). Peroxisome proliferator-activated receptor gamma (PPARγ)-small interfering RNA (siRNA), SREBP2-siRNA, LDLR-siRNA, Scap-siRNA, Insig-1-siRNA, bone morphogenetic protein and activin membrane-bound inhibitor (Bambi)-siRNA, and control-siRNA were from Invitrogen (Carlsbad, CA). Anti-miR33a, pre-miR33a, and control-miR33a were from Ambion (Austin, TX).

Animal Studies. Nine-week-old male C57BL/6J mice (CLEA Japan, Tokyo, Japan) were fed a CE-2 (control; CLEA Japan), CE-2 with 1% cholesterol (HC), methionine-choline-deficient (MCD; Cat. No. 960439; ICN, Aurora, OH), or MCD with 1% cholesterol (MCD+HC) diet for 12 weeks. As another animal model of NASH, 9-week-old male C57BL/6J mice were also fed a CE-2, HC, high-fat (HF; prepared by CLEA Japan according to the #101447 composition of

Received September 30, 2012; accepted June 20, 2013.
Supported in part by a Grant-in-Aid for Scientific Research from the Ministry of Education, Culture, Sports, Science, and Technology of Japan (to K. Tomita)
**These authors contributed equally to this work.*
Address reprint requests to: Kengo Tomita, M.D., Division of Gastroenterology and Hepatology, Department of Internal Medicine, National Defense Medical College, 3-2 Namiki, Tokorozawa-shi, Saitama 359-8513, Japan. E-mail: kengo@ndmc.ac.jp; fax: +81 4-2996-5201.

View this article online at wileyonlinelibrary.com.
DOI 10.1002/hep.26604
Potential conflict of interest: Nothing to report.
Additional Supporting Information may be found in the online version of this article.

Dyets, Bethlehem, PA), or HF with 1% cholesterol (HF+HC) diet for 24 weeks. In the same way, 7-8-week-old C57BL/6 Toll-like receptor (TLR)4-deficient mice (Oriental BioService, Kyoto, Japan) were fed the control, HC, MCD, or MCD+HC diets for 8 weeks or the control, HC, HF, or HF+HC diets for 20 weeks. All animals received humane care in compliance with the criteria outlined in the "Guide for the Care and Use of Laboratory Animals," prepared by the US National Academy of Sciences and published by the US National Institutes of Health.

HSC Isolation and Cell Culture. Wild-type or TLR4-deficient HSCs were isolated from the livers of mice as described.[3] We cultured HSCs on uncoated 6-well plastic tissue culture dishes in serum-depleted Dulbecco's modified Eagle's medium (DMEM), DMEM containing 1% or 10% fetal bovine serum (FBS), and used them as nonpassaged primary cultures or cultures at passage 3-6.

Statistical Analysis. All data are expressed as means (standard error of the mean [SEM]). Statistical analyses were performed using the unpaired Student *t* test or one-way analysis of variance (ANOVA) ($P < 0.05$ was considered significant). When the ANOVA analyses were applied, differences in mean values among groups were examined by Fisher's multiple comparison test.

Results

Increased Cholesterol Intake Accelerates Liver Fibrosis in NASH Without Affecting the Degree of Hepatocellular Injury or Macrophage Recruitment or Activation. Compared with the livers of the MCD diet-fed mice, the livers of the MCD+HC diet-fed mice showed markedly increased centrizonal fibrosis (Supporting Fig. 1A-C). As observed in the MCD diet-induced NASH model, the extent of fibrosis was significantly enhanced in the livers of the HF+HC diet-fed mice, compared with the HF diet-fed mice (Supporting Fig. 1D-F).

HC diet feeding alone was not sufficient to cause liver fibrosis over 12 and 24 weeks (Supporting Fig. 1). In addition, increased intake of cholesterol did not significantly impact hepatocellular damage in the two mouse models of NASH (Supporting Fig. 2). There was no impact on the hepatic messenger RNA (mRNA) levels of Cyp27a1 or on the hepatic content of mitochondrial FC (Supporting Fig. 3).

Similarly, the increased cholesterol intake did not increase macrophage recruitment or activation in either of the two mouse models of NASH (Supporting Fig. 4). Neither did the increased cholesterol intake induce the formation of hepatic macrophage foam cells or cause liver inflammation in these mouse models (Supporting Figs. 1A,D, 5A). In Kupffer cells, there was also no impact on the mRNA levels of Cyp27a1 or on the cholesterol content of both the mitochondria and late endosomes/lysosomes (Supporting Fig. 5B-D). Furthermore, the increased cholesterol intake significantly exaggerated liver fibrosis in Kupffer cell-depleted mice with NASH (Supporting Fig. 6).

FC Accumulation in HSCs Is Enhanced in NASH and Up-Regulates TLR4 Protein Expression and Down-Regulates Bambi mRNA Expression in HSCs. HC, MCD, and HF diet feeding significantly increased FC levels in HSCs compared with the corresponding control diet feeding (Supporting Fig. 7A,D). Further, FC levels were significantly higher in HSCs from the MCD+HC and HF+HC diet-fed groups than in those from the other corresponding groups (Supporting Fig. 7A,D).

The mRNA expression levels of Bambi, the TGFβ pseudoreceptor, were significantly lower in HSCs from the HC, MCD, and HF diet-fed groups than in those from the corresponding control diet-fed groups and in HSCs from the MCD+HC and HF+HC diet-fed groups than in those from the other corresponding groups (Supporting Fig. 7B,E).

HC, MCD, and HF diet feeding increased the amount of TLR4 protein expressed in HSCs. In addition, HSCs from the MCD+HC and HF+HC diet-fed groups showed higher TLR4 protein expression than those from the other corresponding groups (Supporting Fig. 7C,F). No significant difference was observed in the mRNA expression levels of TLR4 among the corresponding groups (Supporting Fig. 7C,F).

HSC Activation in NASH Down-Regulates PPARγ Expression and Enhances Both SREBP2 and miR-33a Signaling; Increased Cholesterol Intake Intensifies These Effects. As noted in the whole livers, the mRNA expression levels of collagen 1α1, collagen 1α2, and α smooth muscle actin (αSMA) were significantly increased in HSCs from the MCD and HF diet-fed groups compared with the corresponding control diet-fed groups. These increases were significantly enhanced by the increased intake of cholesterol (Fig. 1A,D).

The mRNA expression levels of PPARγ1 in HSCs were significantly lower in the MCD and HF diet-fed groups than in the corresponding control diet-fed groups. In addition, these decreases were significantly

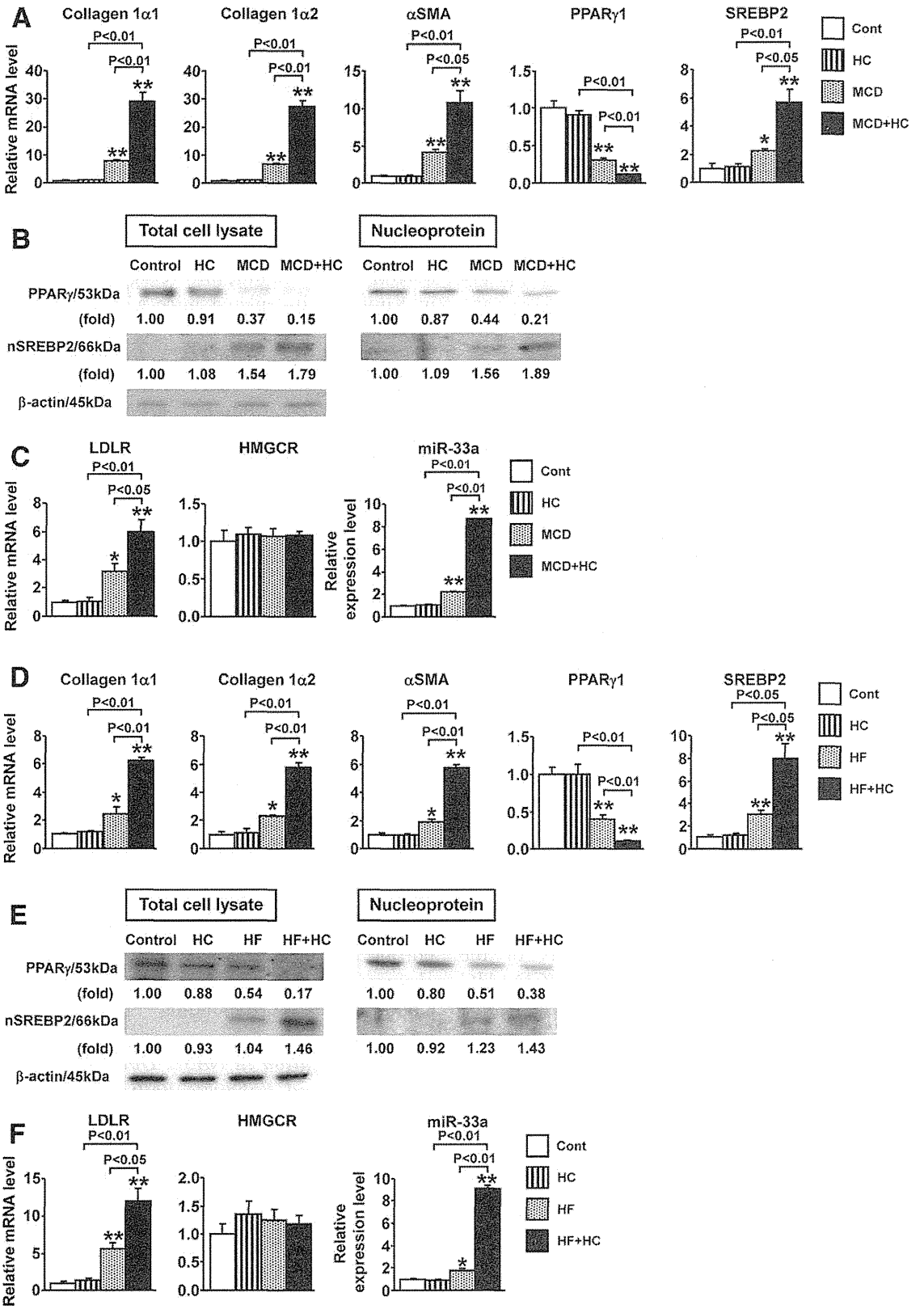

Fig. 1. Down-regulated PPARγ expression and enhanced SREBP2 and miR-33a signaling after HSC activation in the two mouse models of NASH. C57BL/6 mice (9 weeks old, male; n = 6-9/group) were fed (A-C) the control, HC, MCD, or MCD+HC diet for 12 weeks or (D-F) the control, HC, HF, or HF+HC diet for 24 weeks. (A,D) Quantification of collagen 1α1, collagen 1α2, αSMA, PPARγ1, and SREBP2 mRNA in HSCs isolated from the mice in each group. $^{**}P < 0.01$ and $^{*}P < 0.05$, compared with the control diet group. (B,E) Total and nuclear expression of PPARγ and SREBP2 protein in HSCs isolated from the mice in each group. The relative protein levels are indicated below the corresponding bands. (C,F) Quantification of LDLR and HMGCR mRNA, and miR-33a in HSCs isolated from the mice in each group. $^{**}P < 0.01$ and $^{*}P < 0.05$, compared with the control diet group. All data are expressed as means (SEM).

enhanced by the increased intake of cholesterol (Fig. 1A,D). Contrarily, the mRNA expression levels of SREBP2 were significantly higher in HSCs from the MCD and HF diet-fed groups than in those from the corresponding control diet-fed groups, and these increases were significantly enhanced by the increased intake of cholesterol (Fig. 1A,D).

The total and nuclear protein levels of PPARγ were lower in HSCs from the MCD and HF diet-fed groups than in those from the corresponding control diet-fed groups and these decreases were significantly enhanced by the increased intake of cholesterol (Fig. 1B,E). Meanwhile, the levels of the nuclear form of SREBP2 were significantly higher in HSCs from the MCD and HF diet-fed groups than in those from the corresponding control diet-fed groups. Furthermore, these increases were significantly enhanced by the increased intake of cholesterol (Fig. 1B,E).

Similar to SREBP2 expression, the expression levels of LDLR and miR-33a in HSCs were significantly higher in the MCD and HF diet-fed groups than in the corresponding control diet-fed groups. These increases were significantly enhanced by the increased intake of cholesterol (Fig. 1C,F).

In Vitro *HSC Activation Down-Regulates PPARγ Signaling, Which Enhances SREBP2 and miR-33a Signaling.* The total and nuclear forms of PPARγ were abundant in day 1 (quiescent) HSCs but declined in day 3 and 5 (activating) and day 7 (activated) HSCs (Fig. 2A). Meanwhile, the nuclear form of SREBP2 was scarce in day 1 HSCs, and its expression increased at days 3 and 5, and day 7 HSCs (Fig. 2A). Correspondingly, the PPARγ1 and SREBP2 mRNA expression levels were similar to the protein expression levels (Fig. 2A). Furthermore, the expression levels of LDLR and miR-33a in HSCs increased along with their activation (Fig. 2B).

PPARγ-siRNA treatment significantly increased the expression levels of SREBP2, LDLR, and miR-33a in quiescent HSCs (Fig. 2C). Similarly, treatment with the PPARγ antagonist significantly increased the expression levels of SREBP2, LDLR, and miR-33a in quiescent HSCs in a dose-dependent manner (Fig. 2D). On the other hand, overexpression (O/E) of PPARγ1 significantly decreased the levels of SREBP2, LDLR, and miR-33a expression in activated HSCs (Fig. 2E).

SREBP2-siRNA treatment significantly decreased the mRNA expression level of LDLR (Fig. 2F). The addition of PPARγ-siRNA did not affect the mRNA expression level of LDLR in quiescent HSCs treated with SREBP2-siRNA (Fig. 2F).

Enhancement of LDLR Expression and miR-33a Signaling Plays a Role in FC Accumulation in HSCs, Which Subsequently Increases TLR4 Protein Expression Through Suppression of the Endosomal-Lysosomal Degradation Pathway of TLR4. Suppression of LDLR mRNA expression by LDLR-siRNA treatment significantly decreased FC accumulation in HSCs treated with LDL or FBS (Fig. 3A). In HSCs treated with LDL or FBS, FC accumulation significantly decreased with the addition of anti-miR33a and increased with the addition of pre-miR33a (Fig. 3B). Furthermore, FC accumulation in HSCs increased along with their activation (Fig. 3C).

TLR4 protein expression, but not mRNA expression, in HSCs increased along with their activation (Fig. 3D). Treatment with LDL significantly increased TLR4 protein expression in HSCs and suppression of LDLR expression significantly decreased it (Fig. 3E). Similarly, the LDL-induced increase in TLR4 protein expression was significantly suppressed by the addition of anti-miR33a and significantly enhanced by the addition of pre-miR33a (Fig. 3E).

Furthermore, treatment with LDL significantly suppressed the ligand-mediated enhanced degradation of TLR4 in HSCs (Fig. 4A). Both chloroquine, an inhibitor of the endosomal-lysosomal pathways, and MG-132, an inhibitor of the proteosomal pathways, significantly increased TLR4 protein expression in HSCs (Fig. 4B). The addition of LDL did not affect the protein expression levels of TLR4 in HSCs treated with chloroquine, whereas it significantly increased the protein levels of TLR4 in HSCs treated with MG-132 (Fig. 4C,D).

FC Accumulation in HSCs Sensitizes These Cells to TGFβ-Induced Activation Through Enhancement of TLR4-Mediated Down-Regulation of Bambi. The mRNA level of Bambi significantly decreased with LPS treatment, and furthermore, the addition of LDL significantly enhanced the decrease in wild-type HSCs (Fig. 5B). A deficiency in TLR4 signaling reversed these decreases (Fig. 5B).

Wild-type HSCs, pretreated with LPS, demonstrated significant enhancement of collagen 1α1 and 1α2 mRNA expressions when stimulated with TGFβ, and showed a further increase in mRNA expression of collagen 1α1 and 1α2 when treated with LDL (Fig. 5C). A deficiency in TLR4 signaling, however, eliminated these increases (Fig. 5C).

Bambi mRNA expression did not decrease in HSCs treated with LDL, LDLR-siRNA, anti-miR33a, or pre-miR33a in the absence of LPS, but it significantly decreased when HSCs were treated with LPS

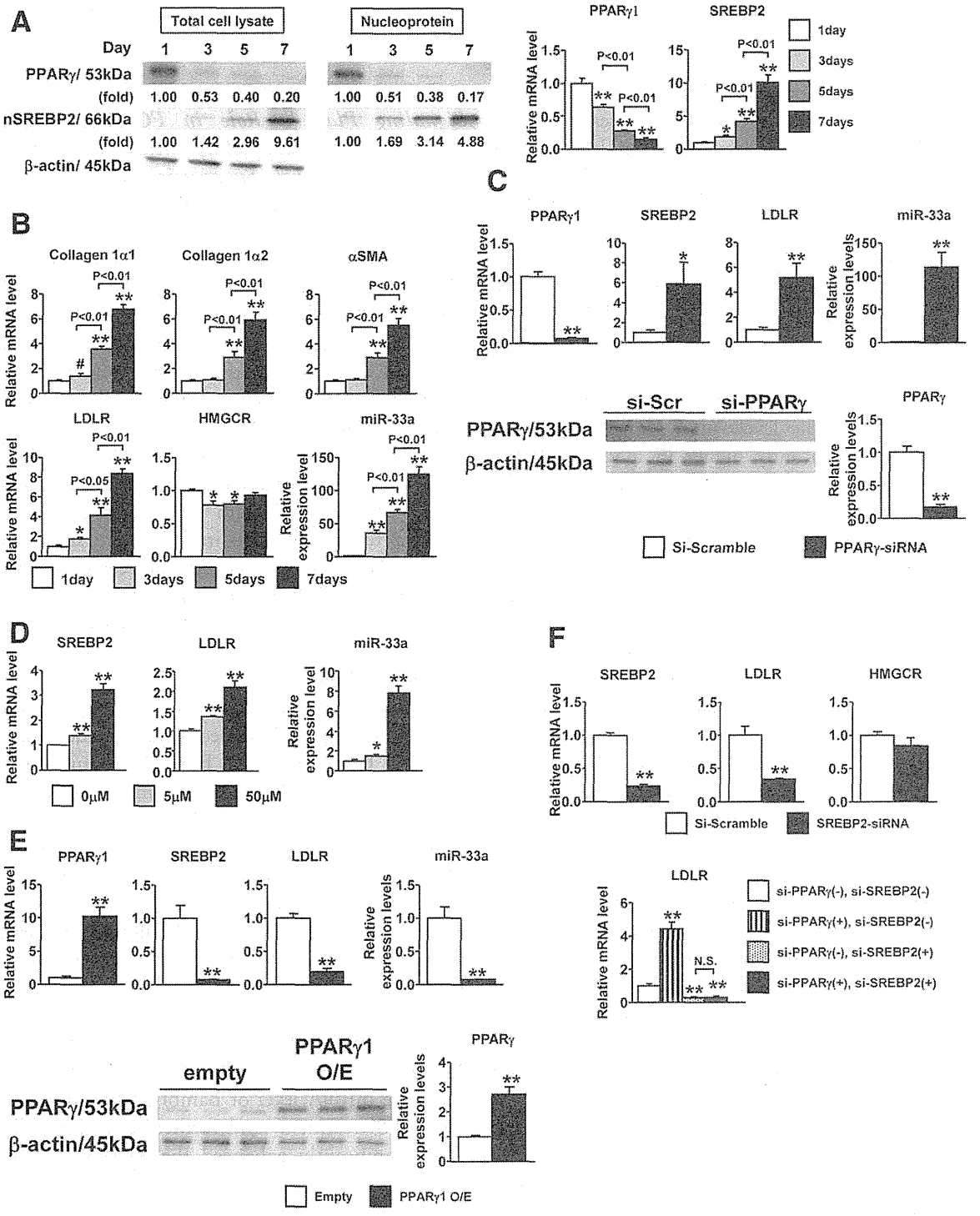

Fig. 2. Down-regulated PPARγ expression and enhanced SREBP2 and miR-33a signaling after HSC activation *in vitro*. (A) Total and nuclear protein expression (left panel) and mRNA levels (right panel) of PPARγ and SREBP2 in HSCs cultured for 1, 3, 5, or 7 days after isolation from C57BL/6 mice. The relative protein levels are indicated below the corresponding bands. $^{**}P < 0.01$, compared with the day 1 culture. (B) Quantification of collagen 1α1, collagen 1α2, αSMA, LDLR, and HMGCR mRNA and miR-33a in HSCs cultured for 1, 3, 5, or 7 days after isolation from C57BL/6 mice. Reflecting the activation of HSCs, the mRNA expression levels of collagen 1α1, collagen 1α2, and αSMA gradually increased from day 1 HSCs to day 3 and 5 HSCs to day 7 HSCs. $^{**}P < 0.01$ and $^{*}P < 0.05$, compared with the day 1 cultures. (C) Quantification of PPARγ1, SREBP2, and LDLR mRNA and miR-33a (upper panel) and PPARγ protein (lower panel) in quiescent HSCs treated with PPARγ-siRNA. $^{**}P < 0.01$ and $^{*}P < 0.05$, compared with the control culture. (D) Quantification of SREBP2 and LDLR mRNA and miR-33a in quiescent HSCs treated with the PPARγ antagonist at the indicated concentrations. $^{**}P < 0.01$ and $^{*}P < 0.05$, compared with the control culture. (E) Quantification of PPARγ1, SREBP2, and LDLR mRNA and miR-33a (upper panel), and PPARγ protein (lower panel) in activated HSCs treated with PPARγ1-O/E vector. $^{**}P < 0.01$, compared with the control culture. (F) Quantification of SREBP2, LDLR, and HMGCR mRNA in activated HSCs treated with SREBP2-siRNA (upper panel). Quantification of LDLR mRNA in quiescent HSCs treated with PPARγ-siRNA and/or SREBP2-siRNA (lower panel). $^{**}P < 0.01$, compared with the control culture. All data are expressed as means (SEM).

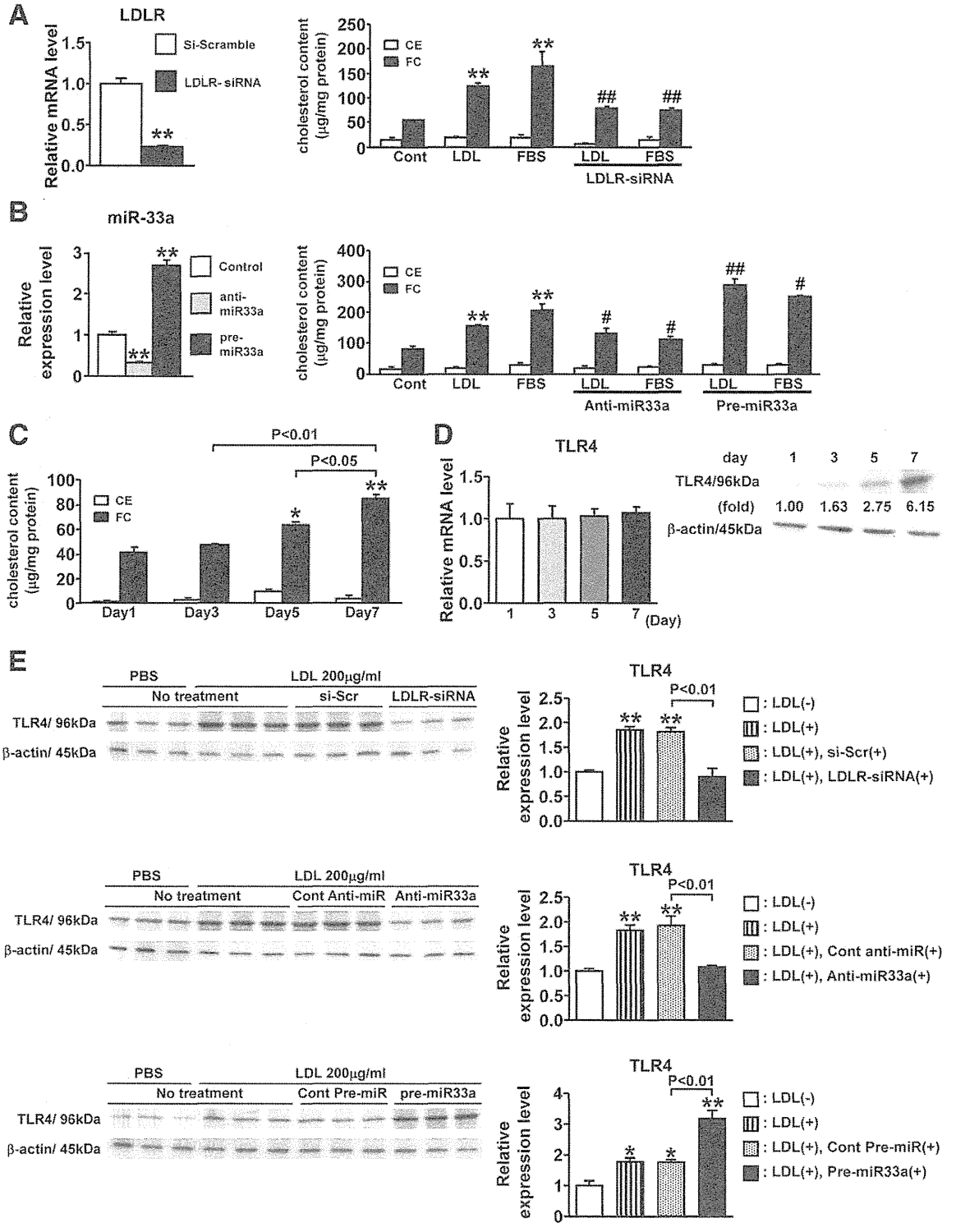

Fig. 3. FC accumulation in HSCs due to enhanced LDLR expression and miR-33a signaling. (A) Quantification of LDLR mRNA (left panel) and cellular FC and CE (right panel) in HSCs treated with LDLR-siRNA in the presence of LDL or FBS. (B) Quantification of miR-33a (left panel) and cellular FC and CE (right panel) in HSCs treated with anti-miR33a or pre-miR33a in the presence of LDL or FBS. $^{**}P < 0.01$, compared with the control culture. $^{\#\#}P < 0.01$ and $^{\#}P < 0.05$, compared with the FC contents in the corresponding cultures without the addition of LDLR-siRNA, anti-miR33a, or pre-miR33a. (C) Quantification of cellular FC and CE in HSCs cultured for 1, 3, 5, or 7 days after isolation from C57BL/6 mice. $^{**}P < 0.01$ and $^{*}P < 0.05$, compared with the day 1 cultures. (D) Quantification of TLR4 mRNA (left panel) and expression of TLR4 protein (right panel) in HSCs cultured for 1, 3, 5, or 7 days after isolation from C57BL/6 mice. The relative protein levels are indicated below the corresponding bands. (E) Expression (left panels) and quantification (right panels) of TLR4 protein in HSCs treated with control-siRNA, LDLR-siRNA, anti-miR33a, pre-miR33a, or control-miR33a in the presence of LDL. $^{**}P < 0.01$ and $^{*}P < 0.05$, compared with the control culture. All data are expressed as means (SEM).